12-2013

Mass production of β-silicon carbide nanofibers by the novel method of Forcespinning

Alfonso Salinas
University of Texas-Pan American

MASS PRODUCTION OF β-SILICON CARBIDE NANOFIBERS BY THE NOVEL METHOD OF FORCESPINNING®

A Thesis

by

ALFONSO SALINAS

Submitted to the Graduate School of
The University of Texas-Pan American
In partial fulfillment of the requirements for the degree of

MASTER OF SCIENCE

December 2013

Major Subject: Mechanical Engineering

MASS PRODUCTION OF β-SILICON CARBIDE NANOFIBERS BY THE NOVEL METHOD OF FORCESPINNING®

A Thesis
by
ALFONSO SALINAS

COMMITTEE MEMBERS

Dr. Karen Lozano
Chair of Committee

Dr. Arturo A. Fuentes
Committee Member

Dr. Horacio Vasquez
Committee Member

December 2013

ABSTRACT

Salinas, Alfonso, Mass Production of β -Silicon Carbide Nanofibers by the Novel Method of Forcespinning®. Master of Science (MS), December, 2013, 52 pp., 3 tables, 40 illustrations, 54 references, 32 titles.

Non-oxide Ceramics such as silicon carbide have very unique properties, for example high toughness, thermal stability, wear resistant, and thermal shock resistance these properties make these ceramic fibers excellent for high temperature applications. Here we present the development of Silicon Carbide nanofibers utilizing a Polystyrene/Polycarbomethylsilane solution as the precursor materials. The Forcespinning® was performed under a controlled nitrogen environment to prevent fiber oxidation. Characterization was conducted using scanning electron microscopy, x-ray diffraction, and thermogravimetric analysis. The results show successful formation of high yield, long continuous bead-free nanofibers with diameters ranging from 280nm to 2 micron depending on the selected processing parameters. The sintered precursors show formation of SiC nanofibers with a beta phase crystalline structure and oxygen content below 15%.

DEDICATION

The completion of my graduate studies would not have been possible without the love and support of my family. My mother, Elvia Salinas, my father, Ildefonso Salinas, my brothers, Marcelo Salinas, Erick J. Salinas, and Graciela Soliz. I would also like to dedicate this to my friends for their support thought my undergraduate and graduate studies.

ACKNOWLEDGMENTS

I will always be grateful to Dr. Karen Lozano, chair of my dissertation committee, for all her mentoring and advice, without her leadership and dedication to the field of nanotechnology, this thesis would not be possible. It has been a privilege working with you and getting to know you. My thanks go to my dissertation committee members: Dr. Arturo A. Fuentes, and Dr. Horacio Vasquez. Their advice, input, and comments on my dissertation helped to ensure the quality of my intellectual work.

I would also like to thank my colleagues from the PREM research group for their unconditional support.

TABLE OF CONTENTS

Page

Page

LIST OF TABLES

Page

LIST OF FIGURES

Page

Page

CHAPTER I

INTRODUCTION

In the past three to four decades a vast number of studies have been conducted on the synthesis and development on 1D nanostructures due to numerous potential applications. These 1D structures include nanofibers, nanowires, nanotubes, and nanoribbons [1]. The development of 1D structures has been accomplished by a variety of methods such as: chemical vapor deposition, electrospinning, liquid vapor grown, carbothermal reduction, arc discharge, laser ablation, plasma torch, and removal of catalyst [2-8].

One of the many 1D structures that has been extensively studied is β-silicon carbide (SiC) given its unique properties such as high mechanical strength, high thermal conductivity, low thermal expansion coefficient good chemical inertness and excellent thermal shock resistance, when compared to those of their bulk counterparts [9]. These unique properties make it an ideal material for ultra-high temperature applications.

β-SiC is also biocompatible and has piezoresistance behavior [10-12]. Specifically, Konttinen et al. studied the possibility of using β-SiC as a ceramic coating of titanium-based hip implant replacement. Their results showed that β-SiC had equal biocompatibility as hydroxyapatite. In the study, a β-SiC coating of about 500 nm thick was applied to titanium pins via ion beam sputtering. β-SiC-coated titanium pins were well tolerated just as uncoated pins,

knowing that titanium is valued as an implant material due to its non-toxicity and mechanical properties [10]. Yang et al. reported for the first time the piezoresistance behavior of a single p-type 6 H-SiC nanowire under different compressed stresses using atomic force microscope (AFM). The piezoresistance coefficient of the nanowire was calculated to be in the range of 51.2 to 159.5 x 10^{-11} Pa^{-1} under applied loading forces ranging from 43.8 to 140.2 nN [11]. Park et al. studied the piezoresistance behavior on a β-SiC micro cantilever transducer. It was confirmed that the dielectric constant of the PZT film improved over 25% [12]. Dimitrijev et al. investigated the piezoelectric response of β-SiC as an energy harvester system for extreme environments; the analysis was conducted via mathematical modeling. The results showed that the output voltage per unit force for SiC is 1.04 times higher than Si and also SiC outperformed Si in extreme environment conditions (above 500 ºC) [13].

Saddow et al. reviewed the major types and the potential applications of SiC for biomedical sensors, such devices require certain chemical, mechanical, and electrical properties when implemented in the harsh environment of the human body. Using SiC in such applications increases the possibility of creating complex devices that can perform multiple biomolecule detection and analysis on a single platform. It is important to mention that the SiC for biological applications is still in the early stages of research, but definitely is a growing area where there is a strong potential for a material with those unique biological characteristics [14]. Varela-Feria et al. demonstrated the use of SiC for biomorphic applications. SiC was developed from pyrolized wood, then liquid silicon filtration, that spontaneously reacted with the carbon to form SiC ceramic. The result was SiC with large concentration of unreacted Si and little unreacted C. In order to remove the unreacted Si a carbon fiber cloth was placed over the SiC/Si composite and cycled at high temperatures to remove the unreacted Si. The SiC ceramics were then exposed to

a final step, coating with bioactive glass. Coating the SiC ceramic with the bioactive glass increased the biocompatibility of the ceramic and increased the biological response of the bone to the implant [15].

Zhu et al. studied β-SiC for a high-strength SiC_w/SiC-Si composite derived after heat treatment using liquid silicon infiltration method. The results showed that the Vickers hardness, flexure strength, elastic modulus, and fracture toughness were 18.8±0.6 GPa, 354±2 GPa, 450±40 MPa, and 3.5±0.3 MPa $m^{1/2}$, respectively. As concluded by the author the high strength properties of the composite was attributed to the β-SiC whiskers. It was also concluded that the unreacted carbon had a negative effect on the mechanical properties [16].

Maboudian et al. grew silicon carbide nanowires by the method of chemical vapor deposition in a SiC thin film of 2 μm. the main objective was to create high temperature supercapacitors. Supercapacitors have attaracted much attention for energy storage applications, having long cycle life and high power densities. Many researchers have develop supercapacitors from nanomaterials like carbon nanotubes, nanowires, or graphene, the lack of this materials resistance to high temperature application makes them unusable. SiC nanowires are ideal for this type of applications given its excellent properties. The authors studied the specific capacitance of the developed SiC nanowires. The authors have demonstrated that the supercapacitor made out of SiC nanowires had a one million cycle lifetime without significant capacitance loss, confirming the potentiality of these nanowires as electrode material for reliable supercapacitors [20]. Yushin et al. studied the behavior of mesoporous CDC material prepared using SiC precursor having ordered mesopores. It was shown that the final product had excellent capacitance retention at high discharge rates. As presented in their results the mesopores had a specific capacitance of 150 F/g for current densities exceeding 17,000 mA/g. It was also

discovered that with the increase of current densities from 1,750-17,500 mA/g, a 2.5% decrease of the capacitance was observed [21].

Lee et al. performed a study on improving the wet contact angle of aluminum with the coating of SiC on carbon nanotubes. The results reveled that not only would improve the contact angles from 145º to 134º, but it will also increase the mechanical properties due to the formation of a covalent SiC bond. Furthermore, the stable SiC layer prevents degradation of carbon nanotubes from the aluminum matrix [22]. Tamari et al. coated MWCNT's (multi-wall carbon nanotubes) with a nanometer-size SiC polycrystalline layer by the reaction of SiO(g) and CO(g). The SiC powders were mixed with MWCNT's and sintered at 1800 ºC. The results showed significant increase in micro hardness and toughness of the SiC coated MWCNT's 30.6 GPa and 5.4 MPa $m^{1/2}$, respectively. It was also shown that the SiC coated MWCNT's had an elastic behavior due to the bridging effect of MWCNT's [23]. Miyamoto et al. performed a similar study as Tamari et al. The authors also coated the MWCNT's to study the oxidation resistance. The coating was performed by the reaction of SiO(g) and CO(g) in vacuum. The sintering process was performed at different temperatures ranging from 1,050 to 1,500 ºC. It was also concluded that the grain size of the SiC can be controlled by the coating conditions. The oxidation durability of the SiC coated and uncoated MWCNT's was tested by heating the samples to 650 ºC and a dwell cycle of 1 hour under an air flow of 50 ml/min. The results revealed that the uncoated MWCNT's were oxidized completely after 5 min, while 70% of the SiC coated MWCNT's stilled remained after 1 hr [24]. König et al. for the first time used electrophoretic deposition to deposit MWCNT's onto SiC fibers to form an effective MWCNT interphase layer for SiC_f/SiC composite. The main purpose of the study was to increase the thermal conductivity and fracture toughness of the composite to enhance the properties of the

SiC_f/SiC composite, to be used in high temperature operation reactors. Research still on going to determine if the MWCNT's that were deposited on the SiC_f/SiC composite had an effect on the thermal conductivity and fracture toughness of these composite materials [25].

Up to date, many studies have been referred to the applications of β-SiC, therefore scientists are researching new and easier methods to develop β-SiC structures. Electrospinning, a cheap and easy set up to develop laboratory scale samples, has been used to obtain SiC precursor nanofibers. In electrospinning, polymer fibers are formed by the creation and elongation of an electric fluid jet. Jiayan et al. electrospun a solution of PVP/TEOS and the authors were able to obtain single-crystalline β-SiC nanowires by carbothermal reduction of the electrospun nanofibers. A carbothermal reduction is a reduction reaction that employs carbon at high temperatures, 1700 °C, in order to reduce the PVP/TEOS nanofibers to β-SiC [17]. Balkus et al. used a preceramic polymer to attempt to decrease the heat treatment temperature; they were able to electrospun SiC nanofibers from a blend of high molecular weight PS/Polycarbosilane with diameters as small as 1 to 2 nm, the smallest as to date. Using a fibrous morphology provides many unique favorable properties; the most important the increase in surface to volume ratio. In order to convert the green SiC nanofibers to SiC, the obtained fibers have to go through a heat treatment process under an inert gas, nitrogen or argon, to prevent oxidation. The X-ray diffraction peaks at 35.2º, 60.2º, and 71.7º corresponded to β-SiC in the [111], [220], and [311] planes of the face-center-cubic [2]. Eick et al. were able to obtain β-SiC fibers (avg diameter of 20 nm) after heat treatment of a blend of PS/PCmS (polycarbomethylsilane). It was determined that the electrospun fibers had an average grain size of 1.25 nm. Eick et al. implemented a step in order to keep the fiber form in the end product, and that was to crosslink the PS to the PCmS via UV light treatment. The green SiC nanofibers were crosslinked for a period of 24 hrs. Something

that is not mentioned in the research article is the distance from the UV light to the green SiC nanofibers, which is important [18]. Chen et al. synthesized PMoCS from a reaction of PSCS with MoCl5 in an argon atmosphere. PMoCS fibers were developed in a lab-scale melt spinning apparatus. The molten polymer was then driven through a filter and spinneret having a single 200 nm capillary tube. The extruded filament was stretched and collected in a rotating spool. The collected fibers were pyrolyzed at different temperatures ranging from 800 ºC to 1600ºC in a nitrogen atmosphere. It was concluded by the authors that below 1000 ºC all of the calcined fibers were α-SiC (amorphous) as showed by XRD results, above 1200 ºC to 1600 ºC β-SiC phase (crystalline) was obtained [6]. Oya et al. also performed a similar study as Chen et al. They synthesized SiC nanofibers from a polymer blend of PS and PCS-XY (Polycarbosilane with 40% Xylene) the blend contained 7:3 ratio, then it was homogenized by stirring after melting at 300 °C in a mixer. The homogenized polymer blend was spun into a melt blown spinning apparatus at 230-250 ºC in argon atmosphere. In this study a new step was introduced, a step that was never mentioned before in the previous studies, it was the stabilization of the developed fibers in air at 200 ºC for 7 hrs. According to the authors the stabilization step is to separate the fibers from each one. The fine fibers were then heat treated to 1000 ºC in an inert atmosphere. As shown by the XRD results, and also according to previous studies the end product was an amorphous silicon oxycarbide. The authors decided to raise the heat treatment temperature to 1500 ºC in order to obtain β-SiC [19]. The previous two studies showed a novel method of developing SiC fine fibers via melt blown processes.

In the many areas that SiC is been developed and researched one of the structures that is been investigated is SiC nanowires as mentioned before. Zhao et al. created SiC nanowires using chemical vapor deposition. The study was focused on the synthesis, structural, and electrical

properties of β-SiC nanowires. The nanowires were synthesized at 1300 ºC. The developed nanowires had a resistivity of 10^{-5}-10^{-4} Ω cm. The results also showed that the nanowires had a high current transport capacity varying from 3 to 15 mA before failure [26].

In all the processes mentioned above to develop SiC nanostructures the amount of material that has been developed is far from been applied in a real world applications and has remained an attractive lab project. The main reason been that the yield produced is way too low, for example, in electrospinning the outcome is about 0.3 g/h [27], furthermore the nanofibers have to go through a pyrolysis process where the material loss is close to 50 wt% depending on the polymer been used, so in reality the yield been produced is only about 0.15 g/h.

Commercial SiC fibers in the micron scale have been produced successfully over the last 30 years. The most common method for producing ceramic fibers is by melt spinning a preceramic polymer followed by heat treatment. SiC based fibers are spun from organic-metallic polymer precursors followed by cross-linking and different heat treatment steps to convert the fiber into ceramic materials. Commercial SiC fibers have also been developed by chemical vapor deposition, which utilizes methyl-trichlorosilane to vapor deposit fine columnar-grained SiC onto a heated carbon monofilament that continuously passes through a long glass reactor. During this process the micron sized fiber go through different changes in physical and chemical properties of the fiber. Hi-Nicalon-S SiC fiber produced by Nippon Carbon from Japan, the first commercially available fiber, uses a production method where the preceramic polymer, polycarbosilane (PCS) is synthesized from dimethyldichlosilane. PCS was spun, followed by crosslinking, and sintering. The fibers had an average diameter in the range of 10 – 20 μm. Two different curing processes where performed, one was thermal oxidation curing at 473 K in air, the second was using irradiation curing with an electron beam. The full development process of

the Hi-Nicalon fibers is shown in Figure 1 [28]. In 1987, Ube Industries another Japanese company publicized the development of their own SiC fiber naming it “Tyranno” which it was derived from polytitanocarbosilane (PTC) precursors. Ube Industries reported that they had better thermal and chemical stability when compared to the other SiC fibers at that time, Nicalon [30].

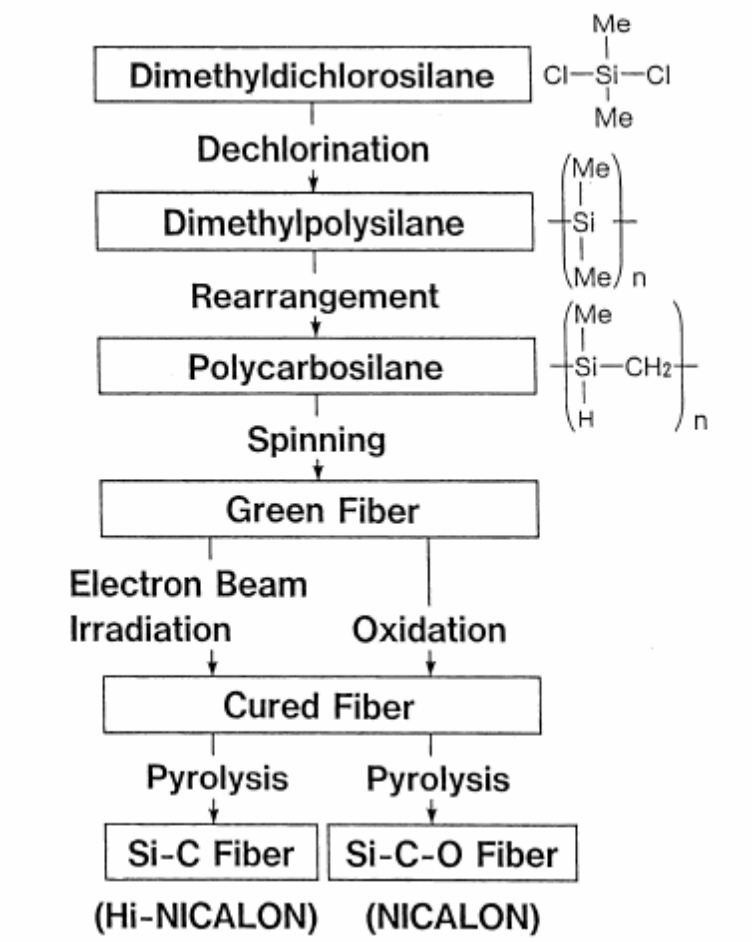

Figure 1. Fabrication Phases of Hi-Nicalon™ and Nicalon™ Fibers [36].

Sylramic another commercial SiC fibers produced by COI Ceramics is also made by a similar process as fibers developed by Nippon Carbon. Specialty materials also develop SiC fiber but using CVD on a 30 μm carbon fiber. The average diameter is about 140 μm regardless of

their large diameter; CVD fibers can show strength up to 6 GPa, when other methods show only 3.2 GPa. Production method of the Specialty materials production method is shown in Figure 2 [29]. Glenn Research Center developed Super Sylramic-iBN, a new type of SiC small-diameter (10 μm) fiber and was given an R&D 100 award in 2001. The development of Super Sylaramic-iBN consists of acquiring the commercial Sylramic SiC fiber (Dow Corning, Midland, MI). The Sylaramic fiber is subjected to a sintering process at high temperatures using boron-sintering aids. The resultant fibers result in very strong fibers (>3 GPa) and also are dense, oxygen free (due to high sintering temperature) and nearly stoichiometric (Si/C = 1) [31]. Table 1, displays the different manufacturers, cross linking method, elemental composition, density, average diameter, and cost from commercially available SiC fibers. Table 2, displays the mechanical properties of commercially available SiC fibers. Oxygen content on the fibers is extremely important. Oxidation of the interface can degrade the fiber or the debonding characteristics of the interface affecting both the strength and the toughness of the ceramics matrix composite (CMC). In order for SiC to be used in high temperature applications (1200-1300 °C) the oxygen content should be less than 10 wt%. Studies have been conducted by previous researchers on oxygen content such as the study done by Steiner et al. where oxygen content was measure to Nicalon, Hi-Nicalon, Nicalon Type S and Sulramic [32]. The results are shown in Table 3. Scanning electron microscope images of Nicalon, Hi-Nicalon, Sylramic and Tyranno are shown in Figure 3 [32-34]. X-Ray Diffraction (XRD) of Sylramic fiber is shown in Figure 4 [32]. Figure 5, shows the XRD spectra of Tyranno SiC fibers that where heat treated at 1300 °C [35]. Figure 6, shows the XRD spectra of Hi-Nicalon and Nicalon SiC fibers [36]. According to data presented by XRD spectra of the four different types of commercial SiC fibers al show the three major peaks at 35.2 °, 60.2°, and 71.7° degrees which correspond to β-SiC with a FCC structure.

Table 1. Commercial SiC fibers (Manufacturer, cross-linked method, composition, etc…) [29].

	Trade mark	Manufacturer	Cross linking method	Approximate maximum production temperature	Elemental composition (wt%)	Density (g/cm^3)	Average diameter (μm)	Cost (US $/kg)
First Gen.	Nicalon 200	Nippon Carbon	Oxygen	1200°C	56Si + 32C + 12O	2.55	14	2000
	Tyranno LOX-M	Ube Ind.	Oxygen	1200°C	54Si + 32C +12O + 2Ti	2.48	11	1250
Second Gen.	Hi-Nicalon	Nippon Carbon	Electron irradiation	1300°C	62.5Si + 37C +O.5O	2.74	12	8000
	Tyranno LOX-E	Ube Ind.	Electron irradiation	1300°C	55Si + 37.5 +5.5O + 2Ti	2.39	11	N/A
	Tyranno ZM	Ube Ind.	Oxygen	1300°C	57Si + 34.5C + 7.5O + 1Zr	2.48	11	1500
	Tyranno ZE	Ube Ind.	Electron irradiation	1300°C	58.5Si + 38.5C + 2O + 1Zr	2.55	11	N/A
Third Gen.	Tyranno SA 1	Ube Ind.	Oxygen	>1700°C	68Si + 32C +0.6Al	3.02	11	N/A
	Tyranno SA 3	Ube Ind.	Oxygen	>1700°C	68Si + 32C +0.6Al	3.1	7.5	5000
	Sylramic	COI ceramics	Oxygen	>1700°C	67Si + 29C +0.8O + 2.3B +0.4N +2.1Ti	3.05	10	10000
	Sylramic iBN	COI Ceramics	Oxygen	>1700°C	N/A	3.05	10	>10000
	Hi-Nicalon Type-S	Nippon Carbon	Electron irradiation	>1500°C	69Si + 31C + 0.2O	3.05	12	13000

Table 2. Mechanical and Thermal Properties of Commercial SiC Fibers [29].

	Trade mark	Manufacturer	Thermal expansion coefficient, ppm/°C (to 1000°C)	Room temperature axial thermal conductivity W/m K	Room temperature strength (GPa)	Room temperature Young's modulus (GPa)
First Gen.	Nicalon 200	Nippon Carbon	3.2	3	3	200
	Tyranno LOX-M	Ube Ind.	3.1	1.5	3.3	185
Second Gen.	Hi-Nicalon	Nippon Carbon	3.5	8	2.8	270
	Tyranno LOX-E	Ube Ind.	NA	NA	2.9	200
	Tyranno ZM	Ube Ind.	NA	2.5	3.4	200
	Tyranno ZE	Ube Ind.	NA	NA	3.5	233
Third Gen.	Tyranno SA1	Ube Ind.	NA	65	2.8	375
	Tyranno SA3	Ube Ind.	NA	65	2.9	375
	Sylramic	COI Ceramics	5.4	46	3.2	400
	Sylramic iBN	COI Ceramics	5.4	>46	3.5	400
	Hi-Nicalon Type-S	Nippon Carbon	NA	18	2.5	400

Table 3. Commercial SiC Fiber Element Composition [37].

Element (wt%)	cg Nicalon	Hi-Nicalon	Nicalon Type S	Sylramic	SiC
Si	56.6	63.7	68.9	66.6	70.0
C	31.7	35.8	30.9	28.5	30.0
O	11.7	0.5	0.2	0.8	
Ti				2.1	
B				2.3	
N				0.4	

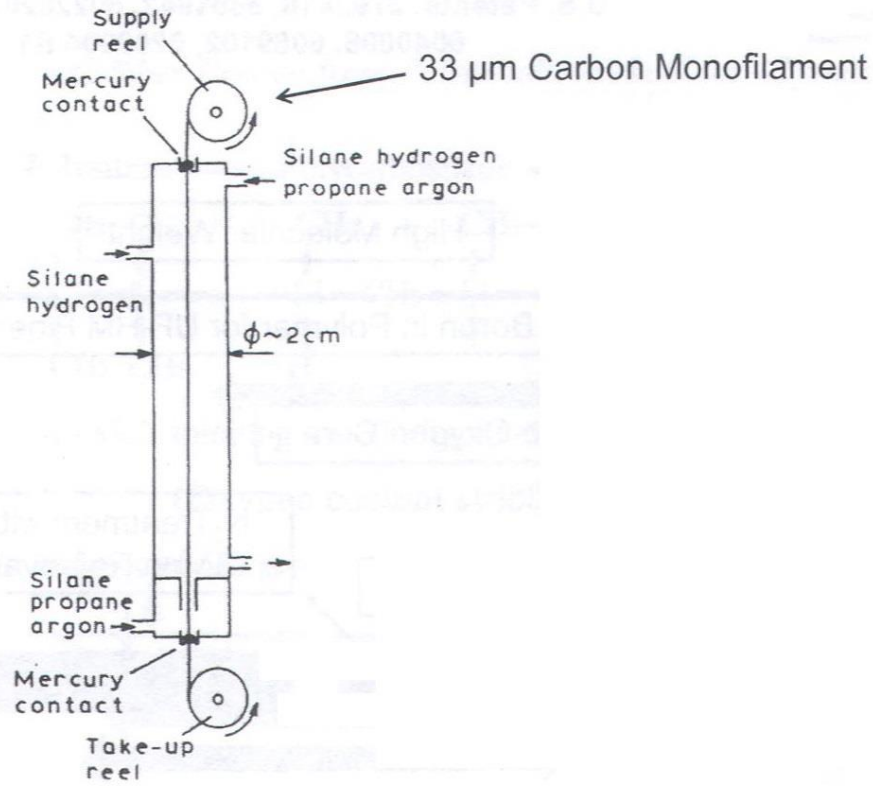

Figure 2. Specialty Materials SiC Fiber Production Process [29].

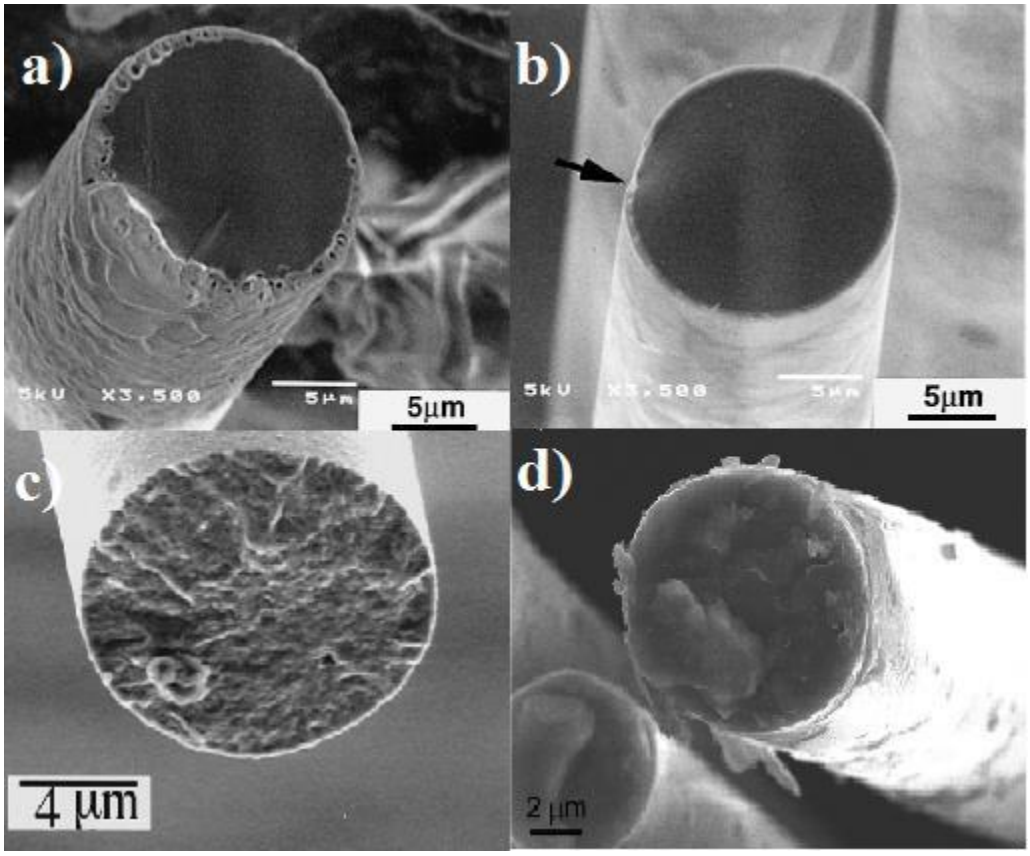

Figure 3. SEM micrographs of a) Nicalon™, b) Hi-Nicalon™, c) Sylramic and d) Tyranno SiC Fibers [36].

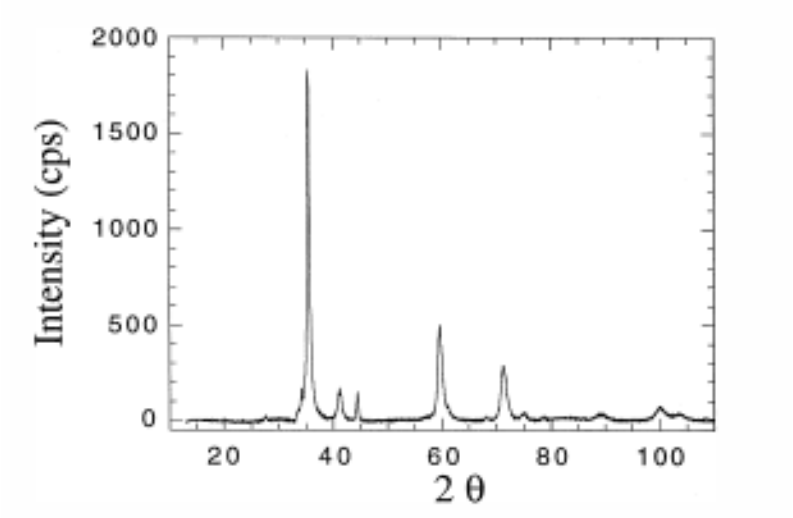

Figure 4. XRD Spectra of Sylramic SiC Fibers [37].

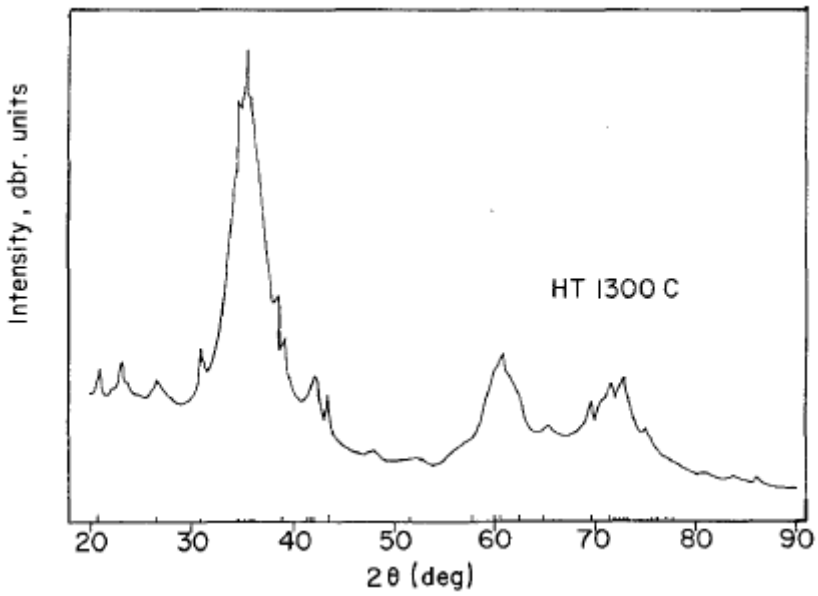

Figure 5. XRD Spectra of Tyranno SiC Fibers [35].

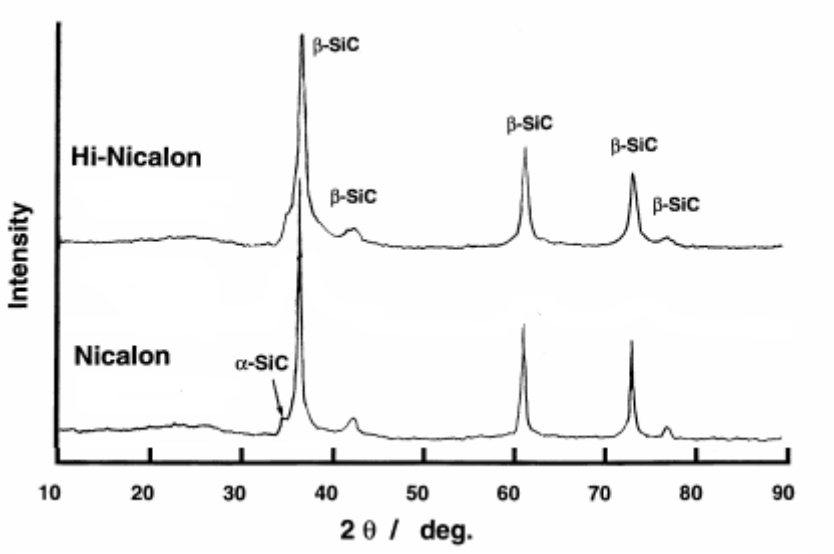

Figure 6. XRD Spectra of Nicalon™ and Hi-Nicalon™ SiC Fibers [36].

This research presents the development of β-SiC nanofibers by the novel method of Focrcespinning® (FS). FS uses centrifugal forces to overcome shear forces and to promote fiber elongation. This newly developed method overcomes the commonly obstacles faced by other

processes such as electrospinning. Conductive and non-conductive solutions or melts can be turned into fiber form given the absence of electric fields. The fiber morphology depends on various factors such as solution viscosity, angular velocity and collector configurations. A yield of more than 1 g/min is usually obtained [27]. The green SiC nanofibers were developed by a process where PS is blended with PCmS and dissolved in an organic solvent to create a polymer solution to be forcespun. The green SiC nanofibers underwent pyrolysis at 1200 °C for a period of 2 hrs under inert atmosphere. The SiC fibers were characterized by FESEM (Field Emission Scanning Electron Microscope), XRD (X-Ray Diffraction), EDS (Energy Disspersive Spetroscopy), and TGA (Thermogravimetric Analysis).

CHAPTER II

EXPERIMENTAL TECHNIQUES

2.1 Scanning Electron Microscope

Scanning electron microscope (SEM), invented by Max Knoll and Ernst Ruska in the 1930's, is a type of microscope that utilizes electrons instead of light to generate an image. When compared to the optical microscope the SEM has much higher resolution typically on the order of 1-2 nm when the instrument is operated between 1 and 30 keV [38]. The SEM various key components in order to operate, this are, electron gun, condenser lenses, various detectors, and a vacuum. A characteristic schematic of an SEM is show in Figure 7. A typical SEM image is shown in Figure 8. The key components of the SEM are described below.

2.1.1 Electron Gun

The electron gun produces a steam of high energy electrons. They are two main types of electron guns, thermionic electron gun and field emission gun. A thermionic gun type is when thermal energy is applied to the filament to move electrons away from the gun and to the specimen been analyzed. Conversely, field emission guns create strong electrical field to pull electrons away from the atoms there are associated with.

2.1.2 Condenser Lenses

The lenses bend the path of the electrons; this produces a clearer and detailed image. These lenses are made of magnets capable of bending the electrons. By bending the electron beam the lenses focus and control the beam directing it to the sample.

2.1.3 Detectors

The detectors are one of the most crucial components of the SEM. The detectors detect the way the electron beam interacts with the sample. The electrons get by the detector, which transforms the electrons into a signal that does get transferred to an amplifier that amplifies the signal to the software to get an actual image.

2.1.4 Vacuum

One of the major draw backs of this instrument is that it has to be under high vacuum (10^{-8} Pa). The reason is that the electron beam generated by the electron gun would interact with air particles in the column. Such interaction would block the path of the electrons to the specimen resulting in a fussy image.

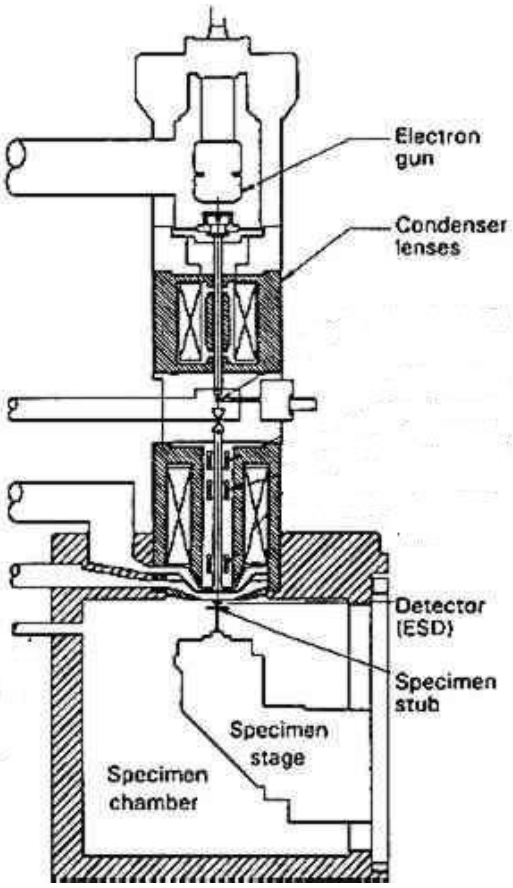

Figure 7. Scanning Electron Microscope [38].

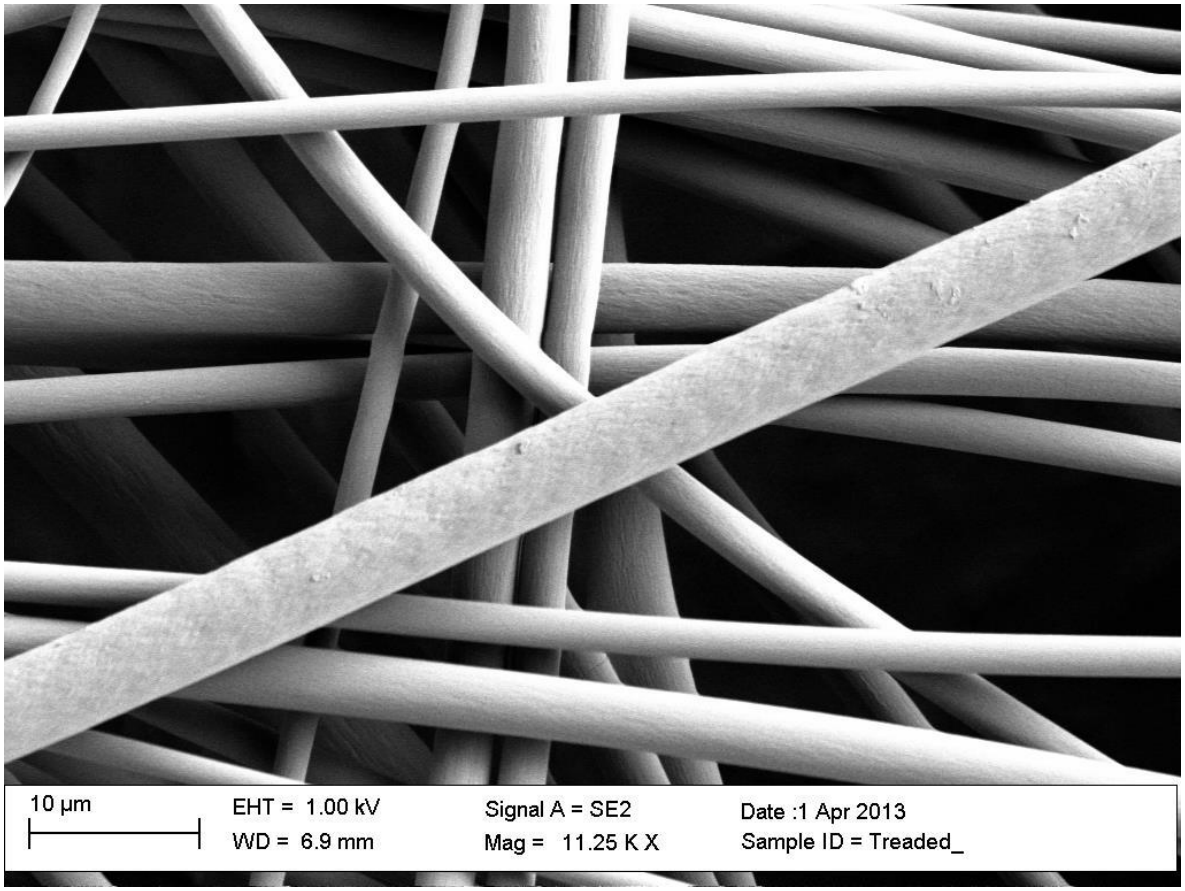

Figure 8. Typical SEM Image of Fibers.

2.2 Thermo Gravimetric Analysis

Thermo Gravimetric Analysis (TGA) is one of the most used instruments in polymeric research. TGA has various components such as furnace, balance, and data acquisition system. A typical TGA experiment consist of heating a sample with a controlled heating rate and recording its weight as increases or decreases under a controlled atmosphere (nitrogen, argon, or air). As the sample is been heated at the selected heating rate, the polymer goes through physical and chemical change. A TGA instrument is presented in Figure 10. The data is displayed in a graph where the Y-axis is displayed as weight (mg) or weight percent (%) and the X-axis is displayed as time (min) or temperature (°C). A typical TGA graph is shown in Figure 9.

2.2.1 Furnace

The main function of the furnace in the TGA is to heat/cool the sample to the wanted temperature at a controlled heating rate.

2.2.2 Balance

The balance weights the sample through the experiment.

2.2.3 Data Acquisition

Data Acquisition system records the temperature and weight loss/gain of the sample as the experiment runs. Thus, the signals recorded can be displayed.

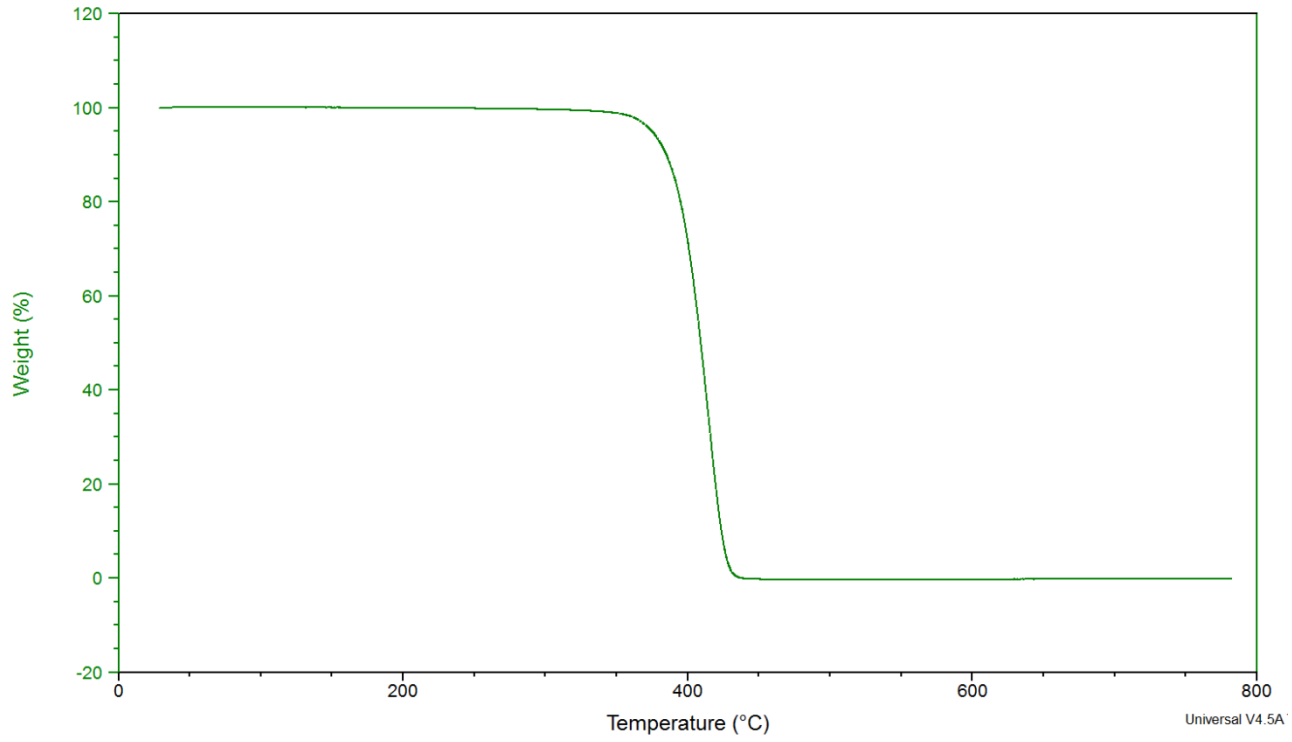

Figure 9. TGA of Polystyrene.

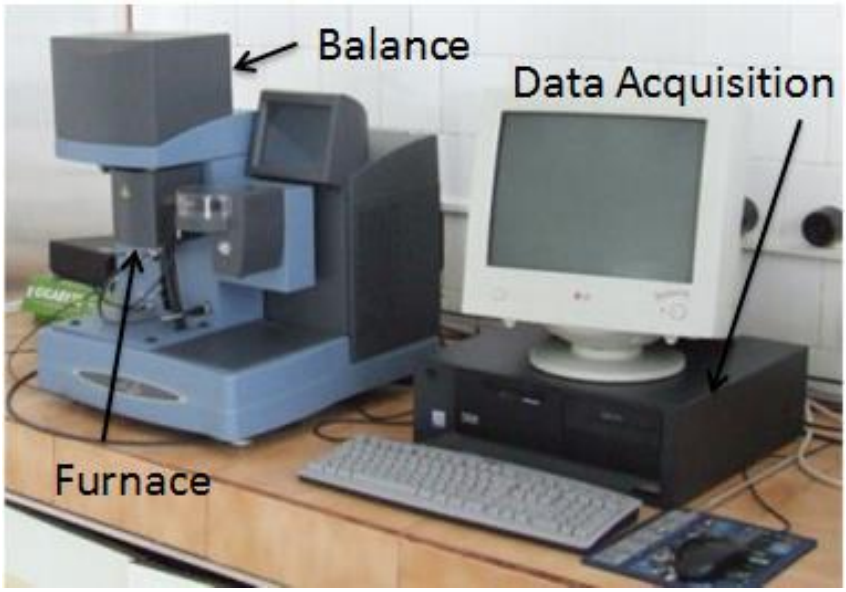

Figure 10. TGA Q500 TA Instrument [39].

2.3 Energy Dispersive Spectrometry

Energy Dispersive Spectrometry (EDS) is an elemental microanalysis method of identifying and quantifying all elements of the periodic table except H, He, and Li. The reason these elements are not detected by the EDS detector is because they are present as major constituents that is, a concentration of C> 0.1 mass fraction [50]. To run such detector an SEM or Transmission Electron microscope (TEM) is required. Characteristic X-rays, which are generated by the interaction of the sample been analyzed and the electron beam of an SEM or TEM that create the x-ray electrons [51]. The most common detectors are made of Si(Li) crystals which operate at low voltages to improve sensitivity The key components of an EDS detector are the entrance window, the Si(Li) crystal, and a field effect transistor (FET) [52]. Figure 11 shows a representation of an EDS detector. Figure 12 shows a typical EDS graph of a sample been analyzed.

2.3.1 Entrance Window

The entrance window maintains integrity of the vacuum and allows transmission of the photos to the crystal.

2.3.2 Crystal

The main function is to absorb the energy of the incoming x-rays ionization, yielding free electrons in the crystal that become conductive and produce an electrical charge bias. The absorption of x-ray converts the energy of individual x-rays intro electrical voltages of proportional size; the electrical pulses correspond to the characteristic x-rays of the element [52].

2.3.3 Field Effect Transistor

The Field Effect Transistor (FET) is placed right behind the crystal and makes electrical contact to the back of the crystal. The FET converts the current pulse into a voltage pulse representative of the original photon energy by acting as voltage regulated capacitor.

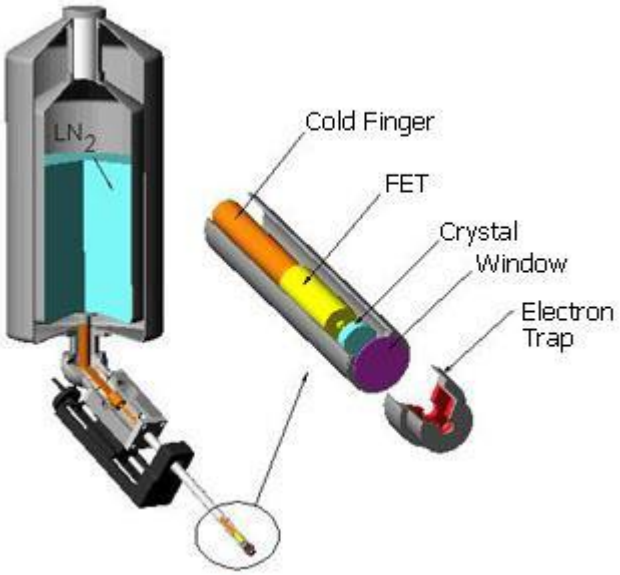

Figure 11. EDS Detector [40].

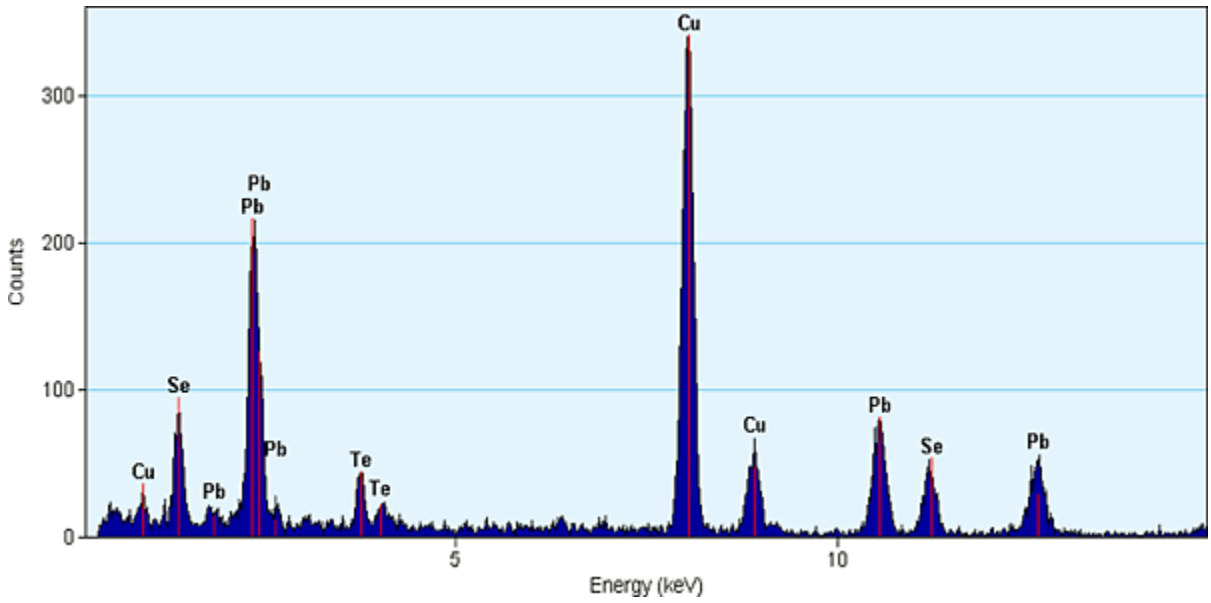

Figure 12. Typical EDS Graph of a Sample [41].

2.4 X-Ray Diffraction

X-Ray Diffraction (XRD) is a technique used to characterize many materials such as metals, polymers, and other compounds. An incident beam of x-rays interfere with atomic planes of a crystal colliding with one another as they leave the crystal. Many properties can be obtained from the XRD including, average spacing between layers or rows of atoms, orientation of a single crystal or grain, find the crystal structure of an unknown material, measure the size, shape and internal stress of small crystalline regions [53]. The XRD consist of three main components the x-ray tube, sample holder and detector. Figure 13 shows a Bruker XRD instruments. Figure 14 displays typical XRD spectra of a crystalline material.

2.4.1 X-ray

X-rays are generated in a cathode tube by heating a filament to produce electrons; the electrons are accelerated towards a sample by applying a high voltage.

2.4.2 Sample Holder

Hold in place the sample been analyzed, two main types of sample holders: reflective and see-through.

2.4.3 Detector

The detector records and process the X-ray signal and convers the signal to a count rate which is then output to a computer [52].

Figure 13. BRUKER D8 ADVANCED XRD Instrument [42].

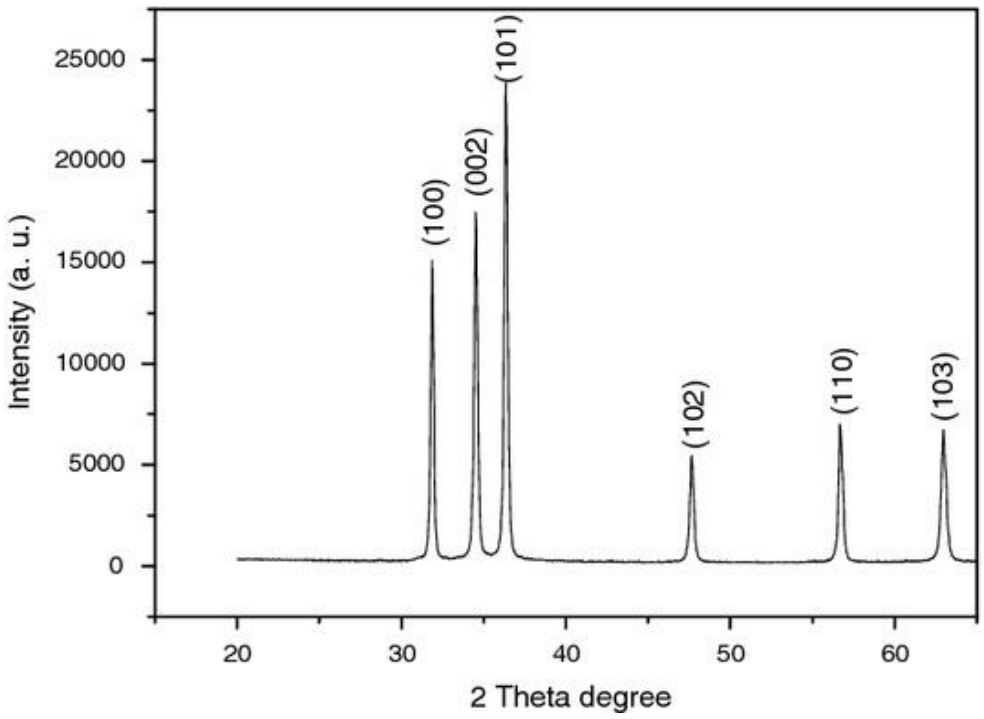

Figure 14. XRD Spectra of ZnO [43].

2.5 Dynamic Mechanical Analysis

Dynamic Mechanical Analysis (DMA) is used to study and characterize mechanical properties as a function of time, frequency, temperature, stress, and/or atmosphere. The material is subjected to sinusoidal force to a sample and analyzing the materials response to that force as shown in Figure 15. The DMA supplies an oscillatory force, causing a sinusoidal stress to be applied to the sample. This generates a sinusoidal strain on the sample. Measuring the amplitude of the sine wave and the lag between the sine waves, modulus, viscosity and damping can be calculated [44]. When characterizing a polymer two major kind of test modes can be used to probe viscoelastic properties: temperature sweep and frequency sweep. A third, but less used is the dynamic stress-strain testing. Figure 16 shows a TA Q800, a DMA instrument. Figure 17 displays a temperature sweep curve obtained using a DMA instrument.

2.5.1 Temperature Sweep

Temperature sweep is when the sample is subjected to a fixed frequency and tested at varying temperatures.

2.5.2 Frequency Sweep

Frequency sweep the sample is subjected to a set temperature and varying frequencies.

2.5.3 Dynamic Stress-Strain

The sample is subjected to amplitude of oscillation of a force. The variation of storage and loss moduli with increasing stress can be used to determine the upper bound of material's linear stress-strain regime [44].

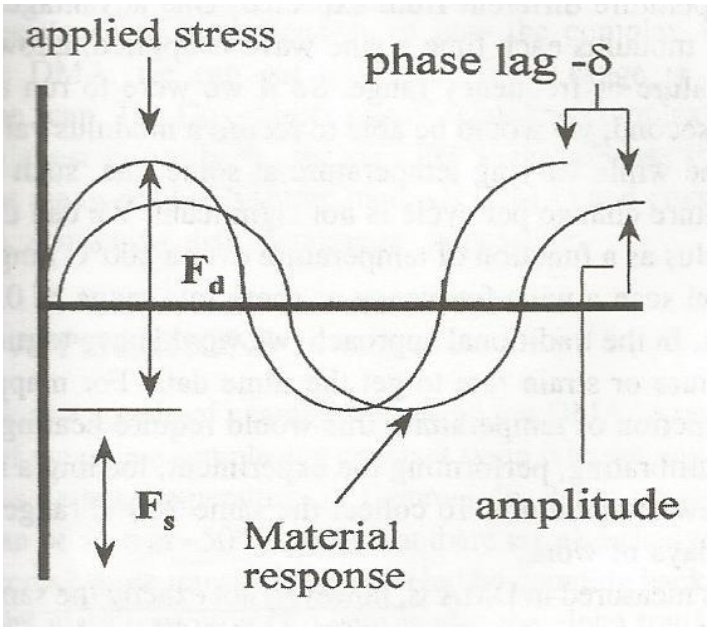

Figure 15. DMA Sine Waves [44].

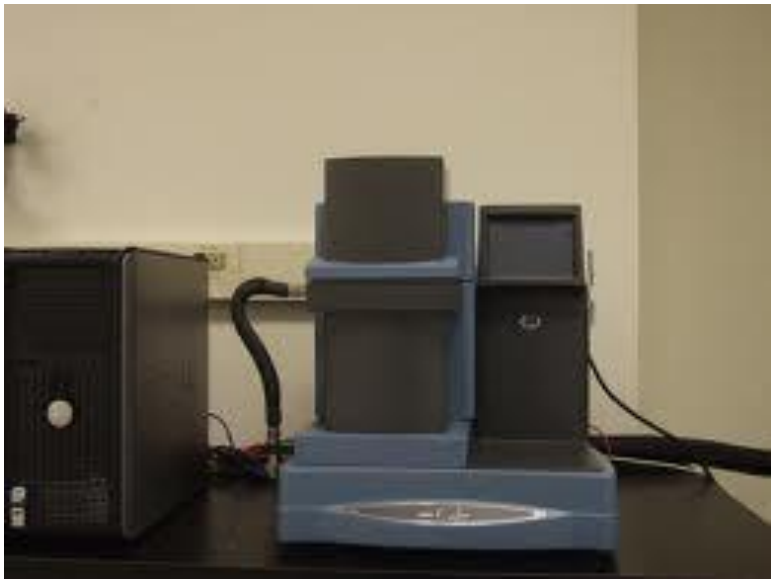

Figure 16. TA Q800 DMA Instrument [45].

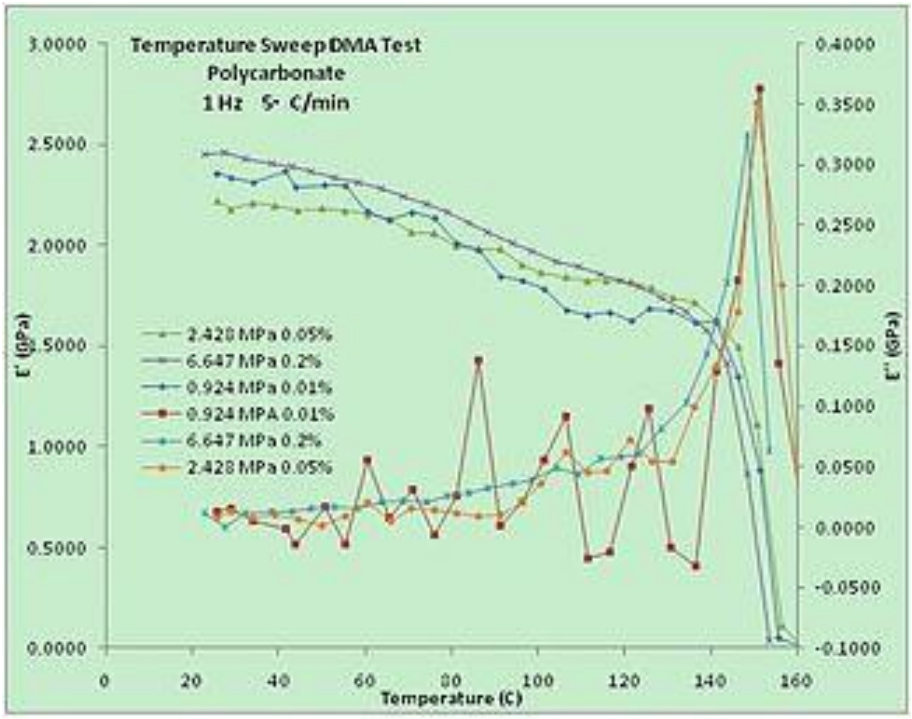

Figure 17. Temperature Sweep of Polycarbonate [46].

CHAPTER III

METHODOLOGY

3.1 Materials

Polystyrene (PS, M_w = 280,000 g/mol) and Polycarbomethylsilane (PCmS, M_w = 800 g/mol) were purchased from Sigma-Aldrich (Milwaukee, WI, USA) and used as received. Toluene was purchased from Fisher Scientific (Waltham, MA, USA) and used as received. The PS/PCmS/Toulene (15, 20, 25 wt% of PS with a 2:1 ratio of PS:PCmS) solutions were prepared inside a MBRAUN (Stratham, NH) glovebox under nitrogen atmosphere in order to prevent oxidation. The solutions were prepared in 20 mL scintillation vials sealed with parafilm, to prevent solvent evaporation, and stirred by magnetic stirrer for a period of 4 hours until fully dissolved.

3.1.1 Material Structure

3.1.1.1 Polystyrene

Polystyrene (PS) an amorphous thermoplastic polymer is used in various applications such as packaging materials, plastic forks, Styrofoam™, pens, etc… PS is produced by free radical vinyl polymerization, from the monomer styrene. PS has a linear molecular formula of $[CH_2CH(C_6H_5)]_n$ or as shown in Figure 18.

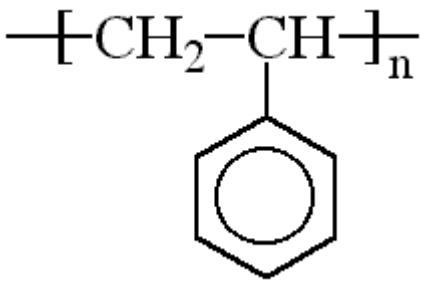

Figure 18. Polystyrene Monomer [47].

3.1.1.2 Polycarbomethylsilane

Polycarbomethylsilane (PCmS) a preceramic polymer used as a silicon source to develop Si structures. PCmS called a "silane" polymer which differs from common polymers such as PS, Polyethylene (PE), Nylon 6, Polypropylene (PP), Polytetrafluoroethylene (PTFE), Polyvinylchloride (PVC) to name a few, by having a silicon (Si) backbone structure, whereas common polymers have a carbon (C) structure. PCmS has a linear molecular formula of $(C_2H_6Si)_n$ or as shown in Figure 19.

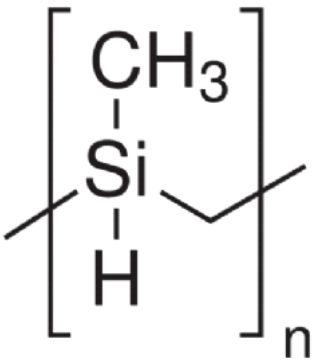

Figure 19. PCmS Monomer [48].

3.2 Forcespinning®

The fibers were produced by the novel technique of Forcespinning® [54]. The Forcespinning® was conducted inside a glovebox under nitrogen environment using a Forcespinning® prototype that was previously modified to fit inside the environmental chamber as shown in Figure 20. Approximately 2 mL of solution was inserted into a cylindrical spinneret using a 10 mL syringe. The spinneret was outfitted with capillary tubes having an inner diameter of 133 μm and 12.7 mm long as shown in Figure 21. The angular velocity at which the fibers were forcespun was varied from 5,000 rpm to 9,000 rpm and solutions were forcespun for 30 sec. The fibers were collected on a circular collector having 16 equally spaced polytetrafluoroethylene (PTFE) bars. The produced fibers were collected using microscope glass slides as shown in Figure 22 and stored inside glovebox in order to prevent fiber oxidation.

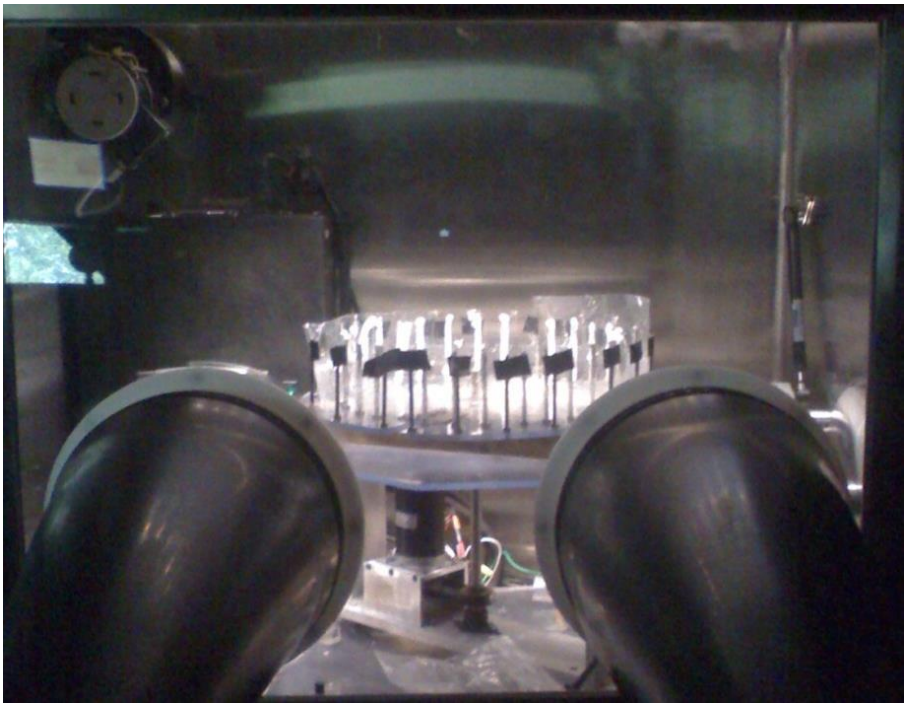

Figure 20. Forcespinning® Apparatus Inside an Environmental Chamber.

Figure 21. Cylindrical Spinneret with Capillary Tubes [49].

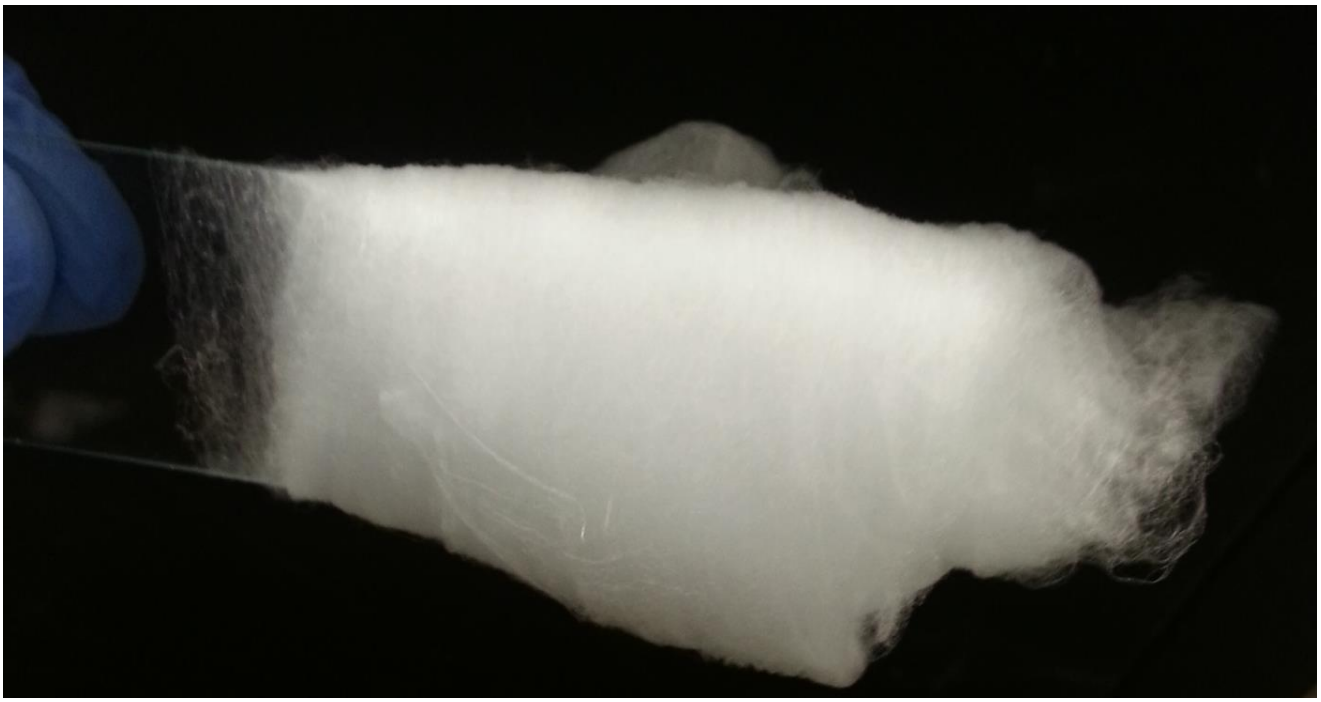

Figure 22. Collected Fibers on Microscope Glass Slide.

3.3 Crosslinking

The collected fibers were placed under a 254-nm wavelength UV light source for a period of 24 hours to crosslink the PS. The crosslinking was performed inside a glovebox under

nitrogen environment to prevent fiber oxidation. Fibers had to be cross-linked because PS reaches the glass transition temperature before the preceramic polymer (PCmS) changes phases from α to a β phase. Crosslinking will cause the fibers to keep the fiber morphology during heat treatment process.

3.4 Heat Treatment

Sintering of the produced fibers after UV light was performed in a CM tube furnace (Bloomfield, NJ, USA) under nitrogen flow of 30 ml/min. The fibers were sintered to a temperature of 1200 °C with a ramping rate of 10 °C/min with a dwell cycle of 2 hours.

3.5 Fiber Characterization

The fibers were characterized using various instruments. Fiber morphology were analyzed using the Carl Zeiss Sigma VP Scanning Electron Microscope (SEM), thermal characterization was performed using a TA Instruments SDT Q600 (DSC/TGA). TGA analysis was performed from room temperature to 1200 °C at a rate of 10 °C/min under nitrogen flow of 30 mL/min. X-ray Diffraction analysis; a Bruker AXS D8 Diffratometer was utilized. The fibers were scanned from a range of 20-80° 2θ angles using a 2D-detector. Dynamic mechanical analysis was performed on the fibers using a TA instruments Q800 DMA with a preload force of 0.001 N and a ramping force of 0.001 mN until the fiber failed.

CHAPTER IV

RESULTS AND DISCUSSION

To optimize the homogeneity, yield, bead free continuous green SiC fibers, the percentage of polystyrene in the polymer solution was increased and decreased 5 wt% of the "working solution" (20 wt%). The 3 polymer solutions (15 wt%, 20 wt% and 25 wt%) were each forcespun at 5000, 7000, and 9000 rpms at room temperature inside a controlled nitrogen environment. After the spinning process, morphological analysis using SEM was performed to evaluate processing effects in fiber diameter and overall fiber structure. Statistical analysis was perfomed over one hundred measurements of each angular velocity and concentration, diameter distribution graphs in Figures 23, 25, and 27. The diameters where measured using Carl Zeiss AxioVision software that was provided by the SEM manufacturer. It was noted by naked eye that the polymer concentration and fiber yield had a positive relationship, as it is shown in Figures 24, 26, and 28. The lowest average diameter is 272.7 nm and it was obtained using a concentration of 15 wt% with an angular velocity of 5000 rpm. The highest average diameter is 2090 nm, and it was obtained using 25 wt% concentration and an angular velocity of 7000 rpm. It is important to note that even though the fibers will shrink under the pyrolysis, it was still desirable to select the lower fiber diameter, though yield was as well a serious consideration therefore, it was decided to select the concentration of 20wt% and an angular velocity of 7000 rpm. These parameters offered an optimum composition between fiber diameter and yield. Figure 29 displays an SEM image of the green 20wt% SiC fibers.

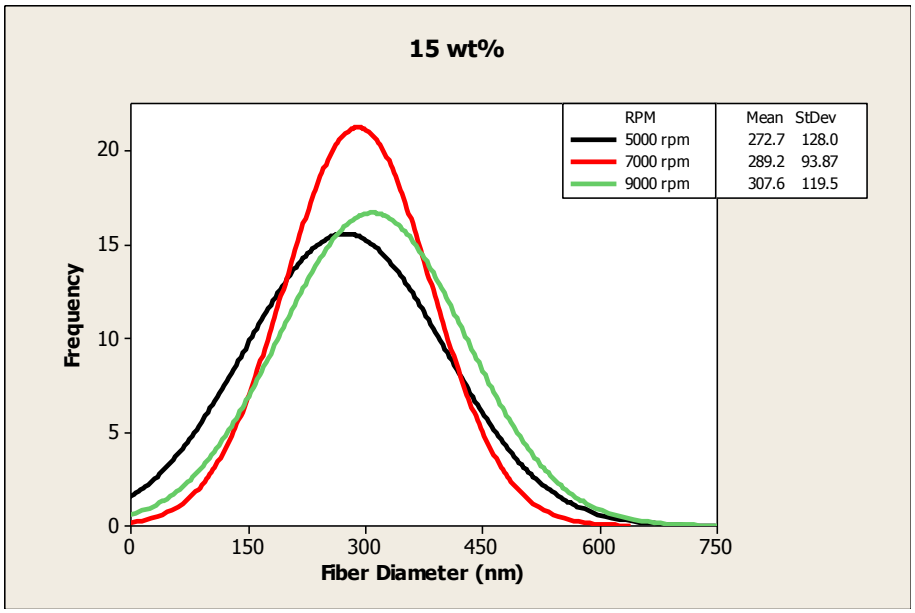

Figure 23. 15wt% Histogram.

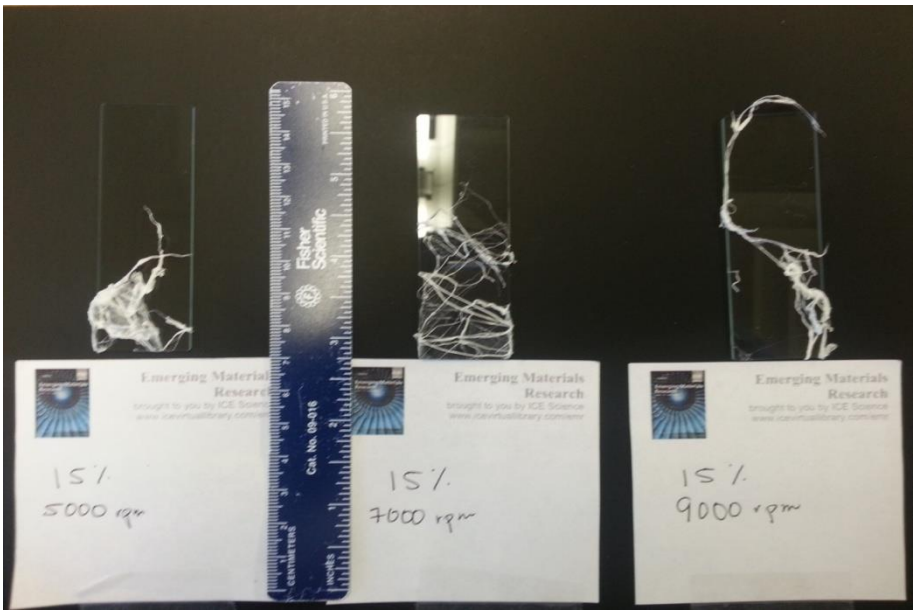

Figure 24. 15wt% SiC Precursors Fibers.

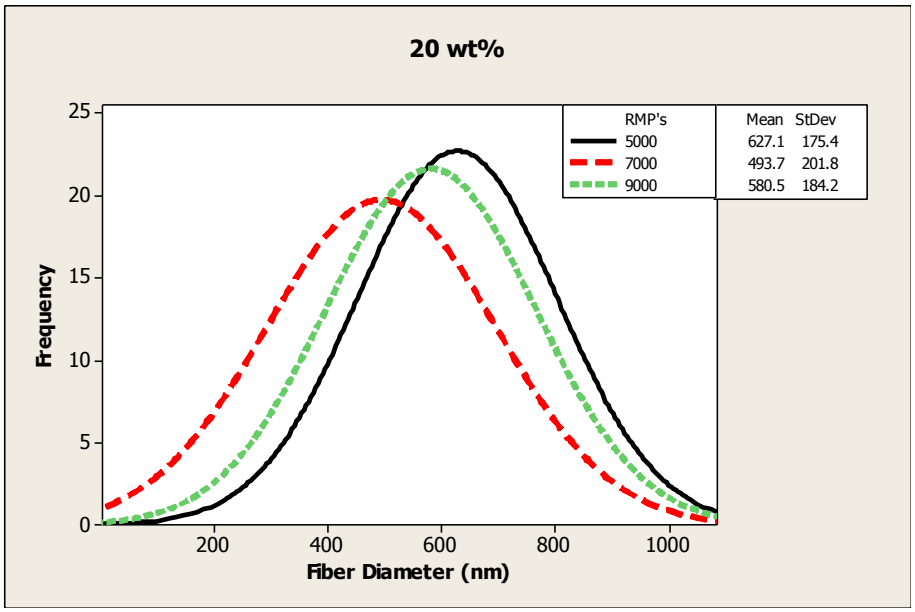

Figure 25. 20 wt% Histogram.

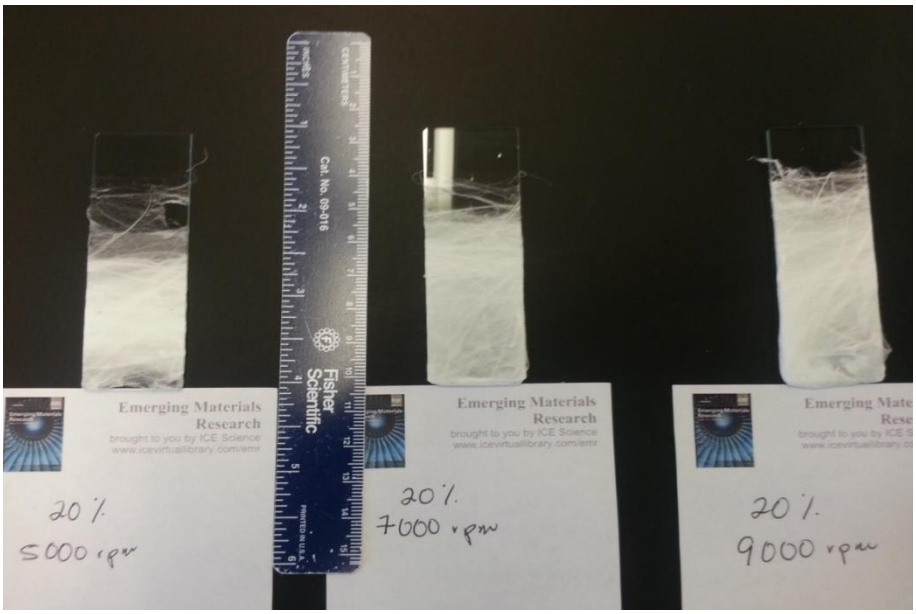

Figure 26. 20 wt% SiC Precursor Fibers.

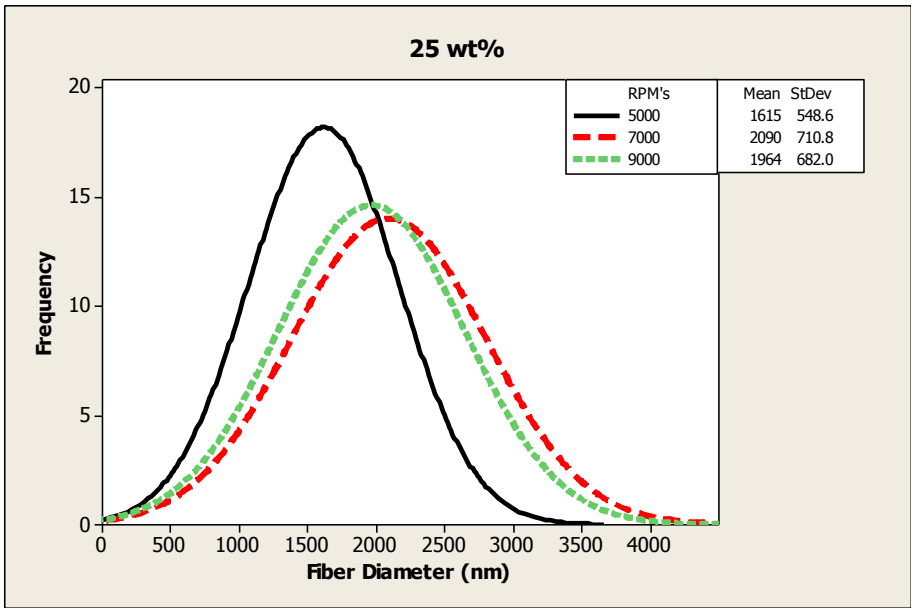

Figure 27. 25 wt% Histogram.

Figure 28. 25wt% SiC Precursor Fibers.

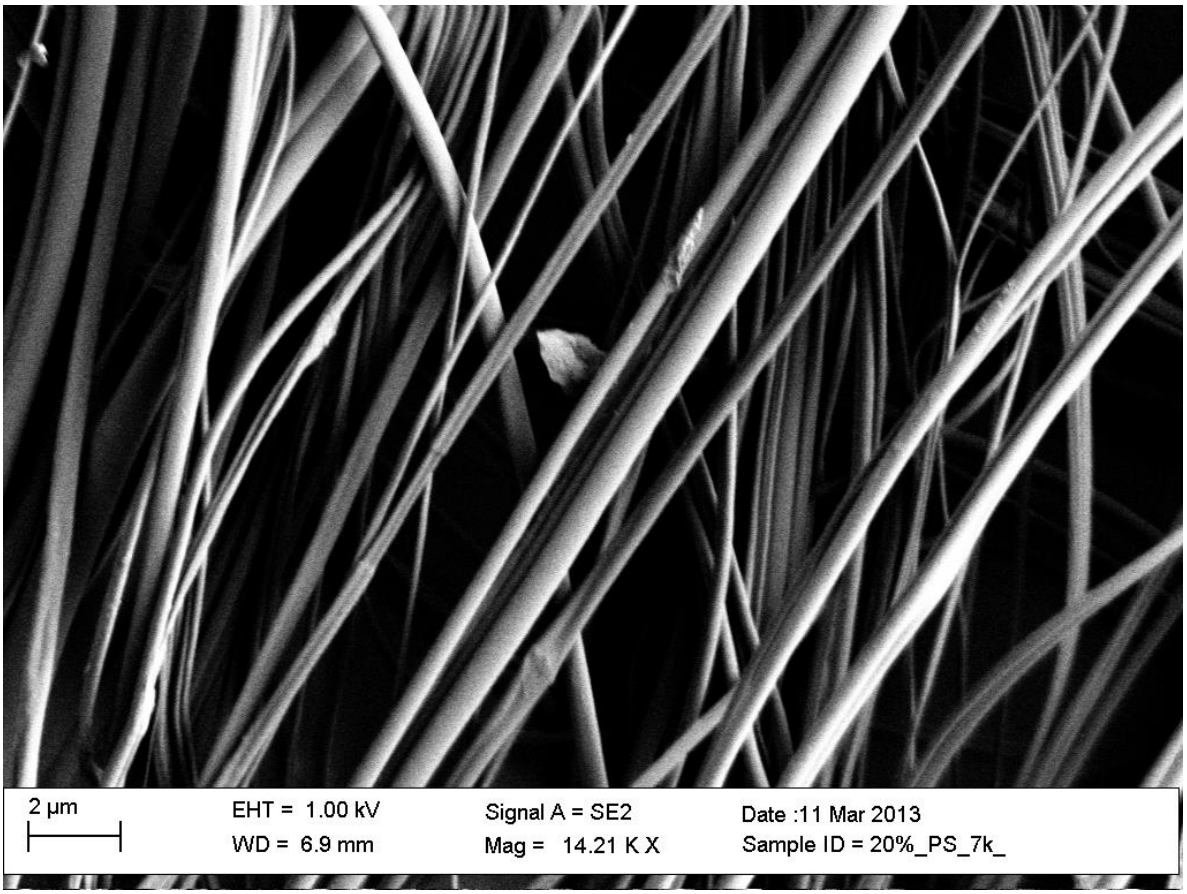

Figure 29. SEM Image of Green SiC Fibers.

As mentioned before, in order to convert the green SiC fibers to SiC, the developed fibers were subjected to a sintering process. The preceramic polymer in this case the PCmS, undergoes a change from an amorphous to crystalline structure at high temperatures. According to Youngblood et al. that temperature is 1175 °C, this temperature was determined through a TGA analysis as shown in Figure 30 [18]. As seen in the TGA graph, the weight loss at 1175 °C corresponds to

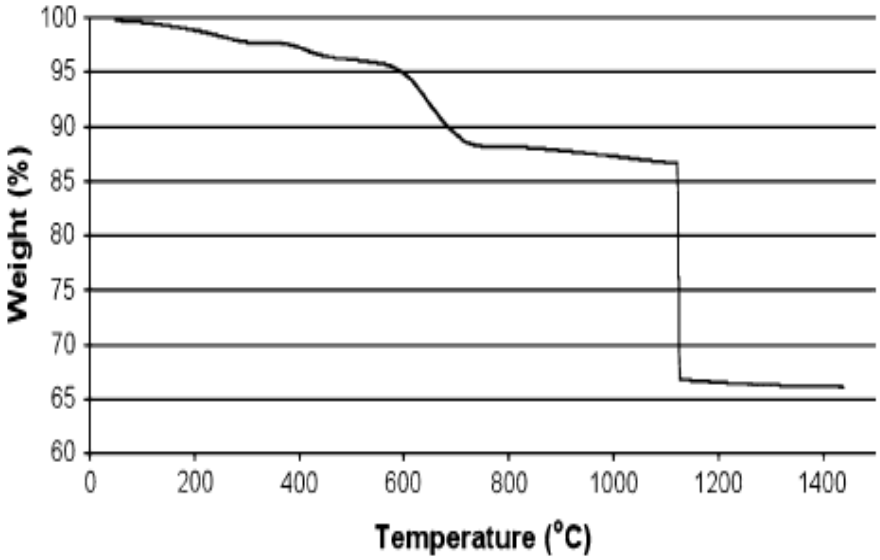

Figure 30. TGA of PCmS [18].

an structural change from amorphous to crystalline according to the Youngblood et al. The developed SiC were subjected to a similar study and results are shown in Figure 9. It should be noted that the results do not correspond to the ones reported by Youngblood et al. The sharp loss that is seen in Figure 30 at 1175 °C is very rare phenomenon, typically when a polymer undergoes a physical or chemical transformation is over a range of temperature and not at one set temperature as reported by Youngblood et al. A typical TGA graph of a common polymer should be very similar to the one shown in Figure 32, where it starts at 100 and ends at 0 weight %, also when the polymer starts to degrade it does not lose weight at a certain temperature it starts to lose weight gradually as seen at Figure 10 at 380 °C. In the case of PCmS, the transition where the polymer turns into a ceramic occurs at a certain temperature, a residue is expected between 600 °C-2730 °C, where 2730 °C is the degradation temperature for SiC [37]. In this research to select the appropriate sintering temperature XRD characterization was performed on

the developed fibers. SiC has diffraction peaks at 35.2 °, 60.2°, and 71.7° degrees which correspond to β-SiC with a FCC structure.

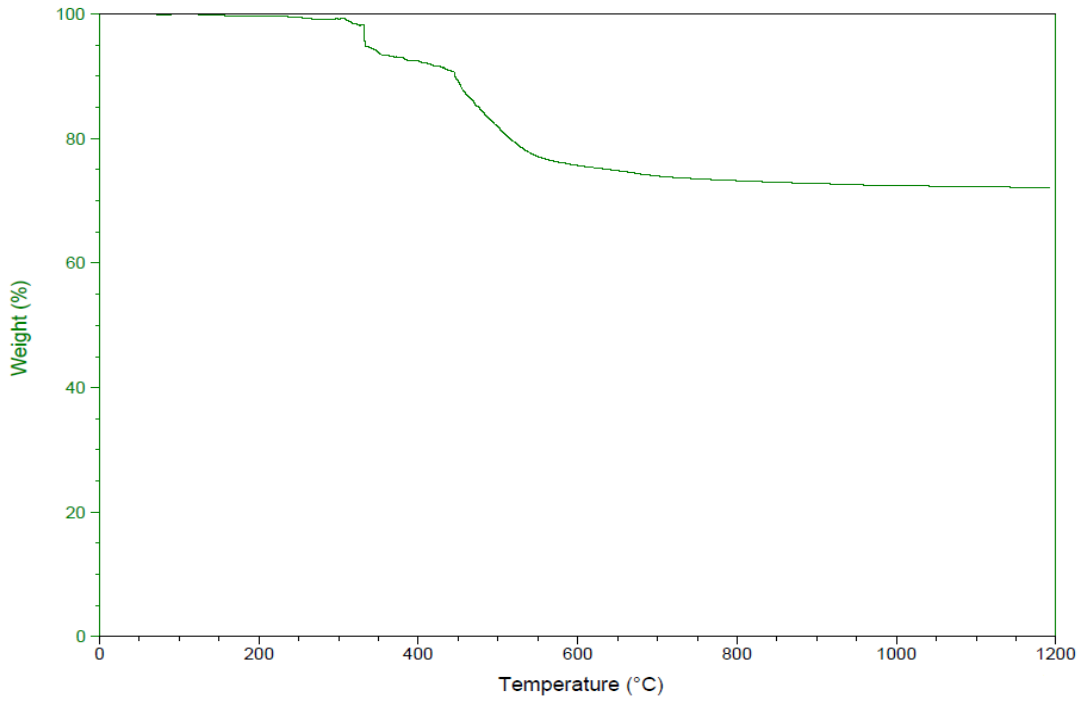

Figure 31. TGA of Our PCmS.

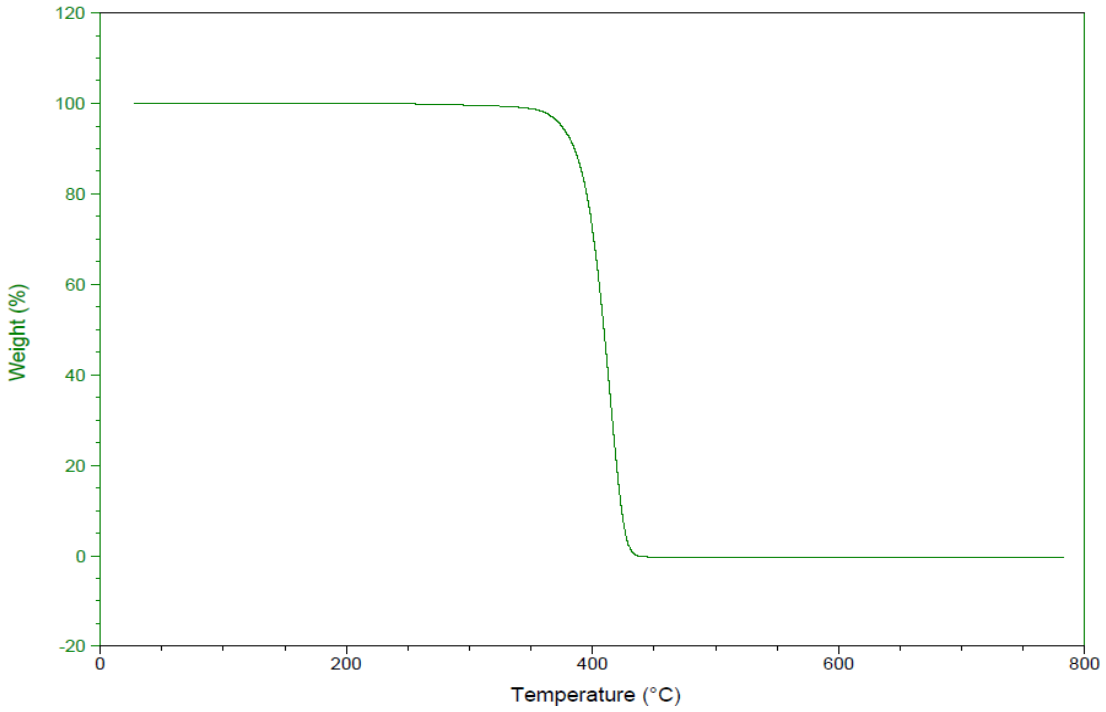

Figure 32. TGA of Polystyrene.

The fibers were exposed to UV light (frequency of 254 nm for 24 hours) before the sintering process in order to promote a crosslinking proces. The main purpose of the crosslinking is to maintain the fiber shape during sintering process; this allows achieving high temperatures and while maintanining fiber shape. Sintering was performed at 1200 °C, using a ramping rate of 10 °C/min and dwell of 2 hours, followed by cooling to room temperature, overall the process was performed under a flow of nitrogen. XRD was performed on the green SiC (G-SiC) and the sintered fibers (1200 °C) as shown in Figure 33, followed by SEM as shown in Figure 34.

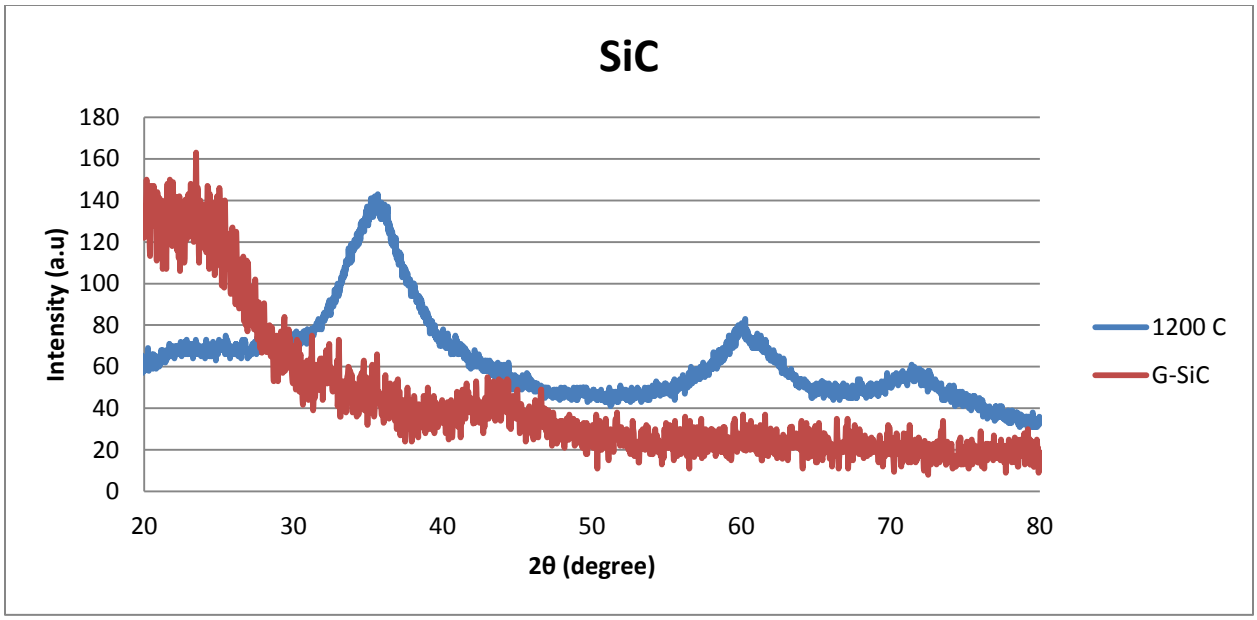

Figure 33. XRD of Green SiC Fibers and Sintered Fibers.

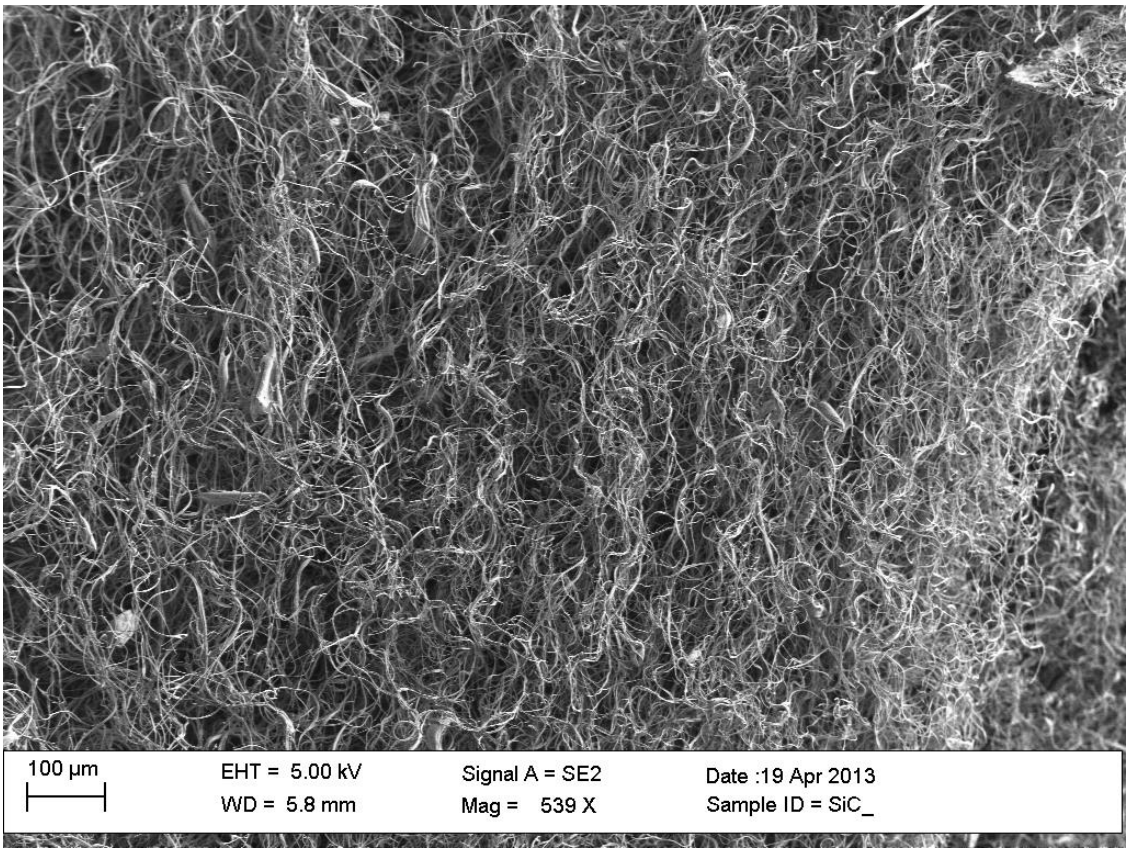

Figure 34. SEM Image of SiC Fibers.

As mentioned in the previous chapter, in order to be considered SiC, the percentage of oxygen present in the fiber has to be less or equal than 10 wt% otherwise is considered silicon oxycarbide (SiOC). Energy dispersive spectroscopy (EDS) was used to measure the chemical composition of the fibers. This technique finger prints the composition of the material with its corresponding chemical content. Figure 35 shows the EDS spectra of the SiC fibers that were sintered at 1200 °C. EDS spectra show the oxygen content in the fibers to be 42.59 wt%. This O content is way too high when compared to the commercially available SiC. At this point it was necessary to track down where the fibers were the oxygen. At every step of the experiment an EDS study was conducted.

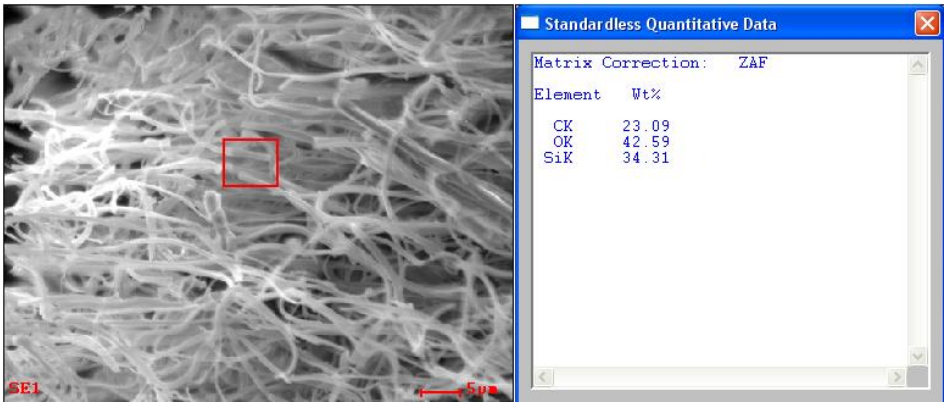

Figure 35. EDS of SiC Fibers Sintered at 1200 °C.

The first step to be evaluated was the polymer solution. A drop of the polymer solution was placed in a SEM stub and dried inside an environmental chamber overnight, Figure 36 shows the EDS results. As the results show the oxygen content is 25.4 wt%. Results show 3.76 wt% of aluminum, that corresponds to the SEM sample holder.

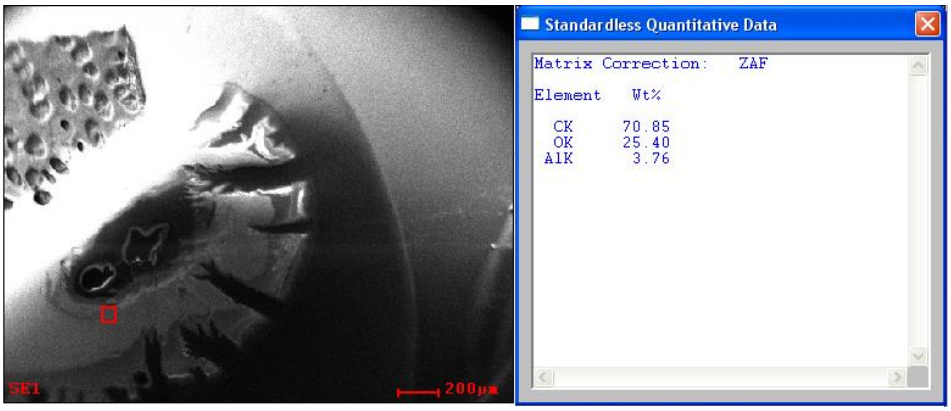

Figure 36. EDS of Polymer Solution.

The second step in the experiment was the development of the green SiC fibers through Forcespinning®. The same conditions were used as the one used to dry the solution. Figure 37, shows the EDS results for the green SiC fibers. The results show that the oxygen content is 13.38 wt%. From the solution to the green SiC the oxygen content decreased by 12 wt%. This is due to the Forcespinning®, because of solvent evaporation.

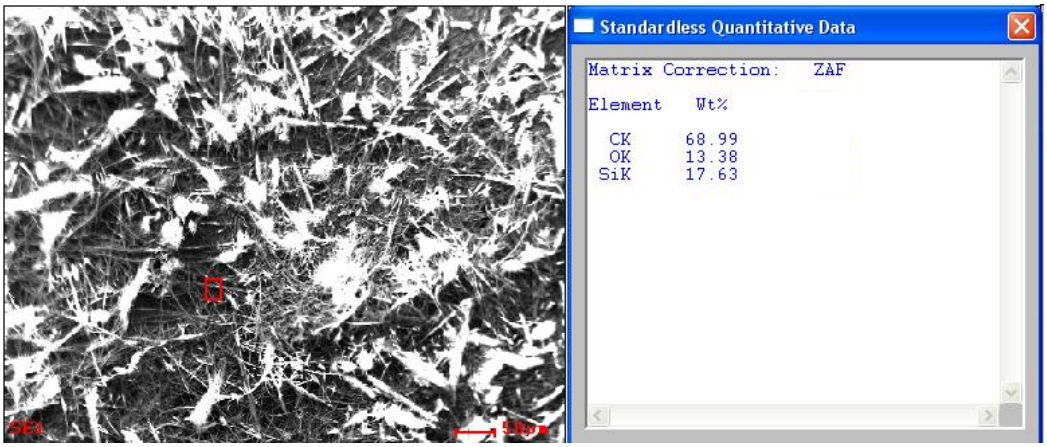

Figure 37. EDS of Green SiC Fibers.

The final step in the experiment was to sinter the fibers at 1200 °C. Figure 38, shows the EDS results for the sintered fibers. After sintering the percentage of oxygen was 48.58 wt%, the

oxygen content in the fibers increased from 13.38 wt% to 48.58 wt% during the sintering process, an increment of almost 35.2 wt%.

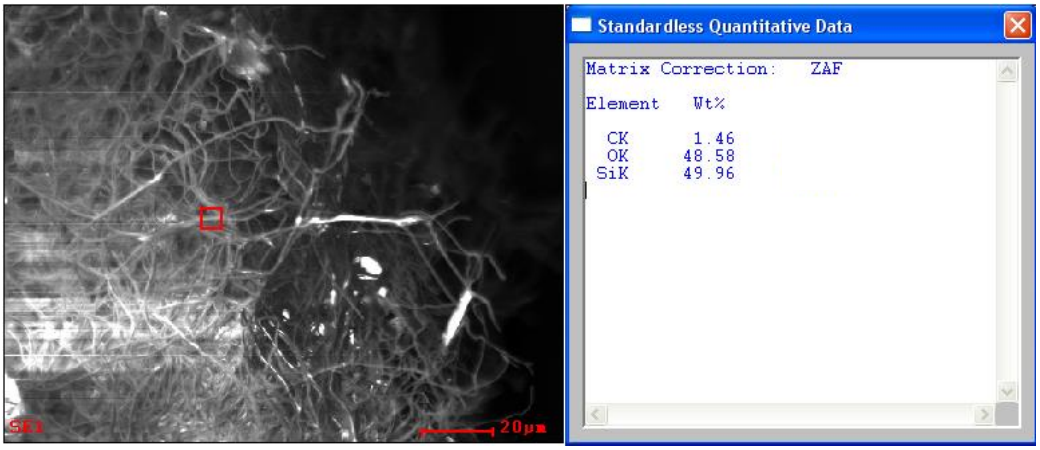

Figure 38. EDS of Sintered Fibers at 1200 °C.

The challenge was now to decrease the amount of oxygen in the SiC fibers during the sintering process. It was decided to cover the green SiC fibers with carbon powder before placing them in the alumina tube furnace. This step promoted an interaction with the carbon instead of the oxygen in the atmosphere. Carbon was sprinkled to the green SiC fibers before sintering, and then the fibers were sintered at 1200 °C. Figure 39 shows the results obtained from the EDS, it can be observed that the carbon that was deposited on the green SiC fibers had an effect on the oxygen content. The oxygen content decreased from 48.58 wt% to 4.33 wt%. The added step reduced the amount of oxygen in the fiber by 44.25 wt%.

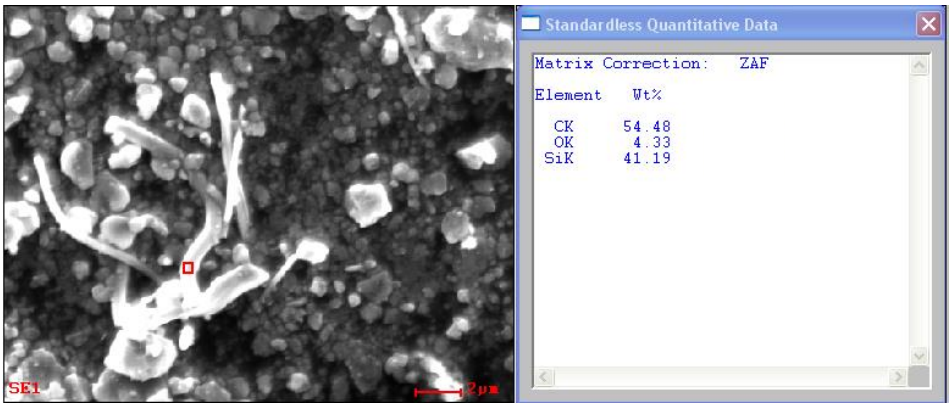

Figure 39. EDS of SiC Fibers After Carbon was Deposited on the SiC fibers.

Different temperatures were studies to observe the change in crystallinity via XRD, five different temperatures were studied, 1100 °C , 1200 °C, 1300 °C, 1400 °C, and 1500 °C. Figure 40, shows the XRD results of the five different sintering temperatures. It can be observed that the crystallinity increased as the sintering temperature was increased.

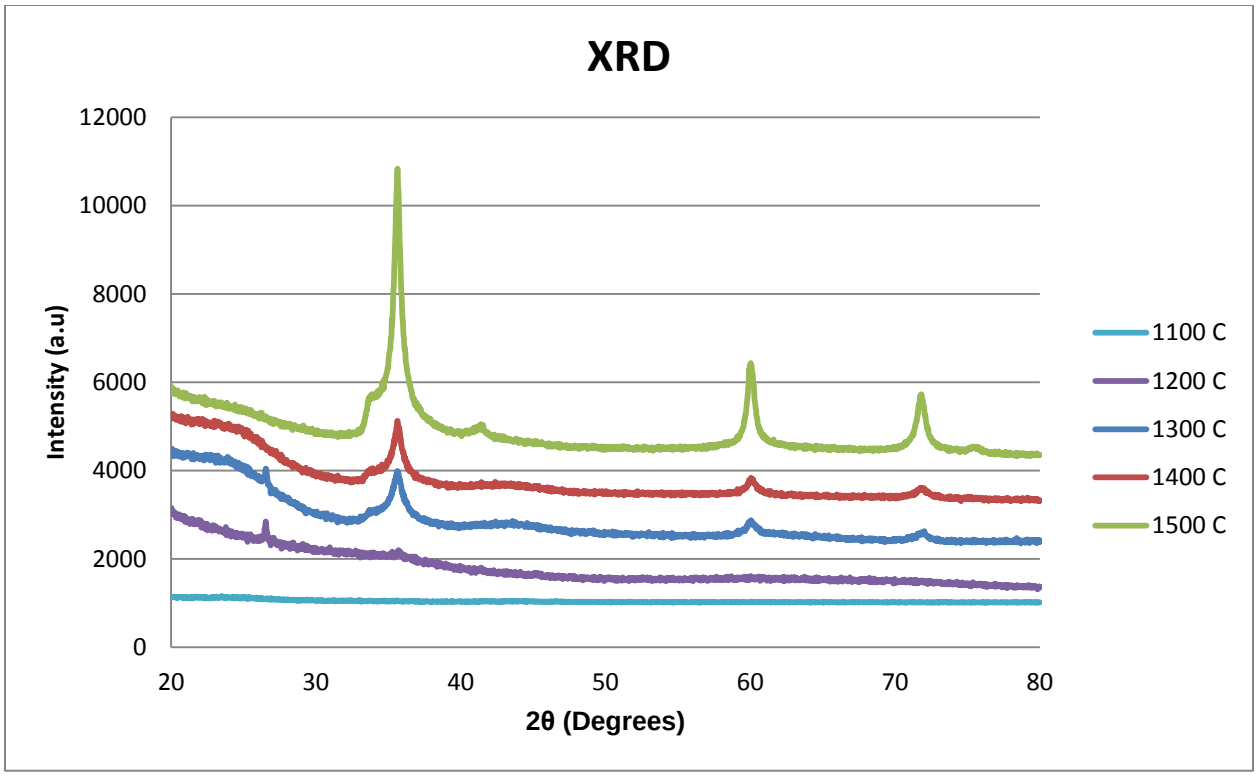

Figure 40. XRD Spectra of SiC Fibers Sintered at Various Temperatures.

CHAPTER V

CONCLUSIONS AND FUTURE WORK

The Forcespinning® technology was utilized to develop SiC nanofibers for potential uses in high temperature applications. The green SiC nanofibers were developed from a polymeric solution blend of PS/PCmS dissolved in toluene following a sintering process at 1200 °C to convert them into SiC. The study found that PS concentration and angular velocity had the most noticeable effect on fiber diameter and yield. The optimum parameters to develop the fiber precursors using the Forcespinning® method were found to be (1) a solution of 20 wt% PS and (2) an angular velocity of 7000 rpm. These parameters produced fibers with the best diameter to yield ratio. It was observed that during the sintering process the fibers oxidize the most, therefore additional steps where conducted to prevent fiber oxidation such as spinning under inert atmosphere, and adding carbon powder to the green SiC fibers. XRD results show that the temperature used to convert the precursors had a significant effect on crystallinity. As it was shown in the present work, as temperature was increased the amorphous phase decreased, increasing the crystallinity of the fibers. This can be seen from the XRD spectra peaks, the peaks start to narrow and increase in intensity as the temperature was increased. Overall, Forcespinning® proves to be a revolutionary successful method in the production of long, continuous, and homogenous SiC nanofibers at a higher yield than previously used methods.

In addition to the research presented above, the author would like to expand on this project. Some of the possible amendments to the experiment that the author is planning to possibly conduct are to incorporate well-aligned multi-wall carbon nanotubes in order to increase the mechanical and electrical properties of the material. Also, use higher rotational speed in order to fully understand the behavior of nanofibers at a higher angular velocity.

REFERENCES

1. Li, X., Chen, X., & Song, H. (2011). Preparation of silicon carbide nanowires via a rapid heating process. *Materials Science and Engineering: B*, *176*(1), 87–91. doi:10.1016/j.mseb.2010.09.007
2. Liu, H. a., & Balkus, K. J. (2009). Electrospinning of beta silicon carbide nanofibers. *Materials Letters*, *63*(27), 2361–2364. doi:10.1016/j.matlet.2009.08.009
3. Xie, Z., Niu, J., & Chen, Z. (2012). Synthesis and characterization of molybdenum-modified polycarbosilane for SiC(Mo) ceramics. *Journal of Applied Polymer Science*, n/a–n/a. doi:10.1002/app.38344
4. Zheng, C.-S., Yan, Q.-Z., & Xia, M. (2012). Combustion synthesis of SiC/Si3N4-NW composite powders: The influence of catalysts and gases. *Ceramics International*, *38*(6), 4549–4554. doi:10.1016/j.ceramint.2012.02.032
5. electronic structure, optical properties and electronic conductivity of silicon carbide nanowires.pdf. (n.d.).
6. Li, X., Chen, X., & Song, H. (2011). Preparation of silicon carbide nanowires via a rapid heating process. *Materials Science and Engineering: B*, *176*(1), 87–91. doi:10.1016/j.mseb.2010.09.007
7. Deposition, C. C. V. (2013). Synthesis and Growth Mechanism of SiC/SiO 2 Nanochains Heterostructure by Catalyst-Free Chemical Vapor Deposition, *633*, 627–633. doi:10.1111/jace.12005
8. Gu, X., Qiang, Y., & Zhao, Y. (2011). Synthesis, structural and electrical properties of SiC nanowires via a simple CVD method. *Journal of Materials Science: Materials in Electronics*, *23*(5), 1037–1040. doi:10.1007/s10854-011-0543-2
9. Huang, Z.-M., Zhang, Y.-Z., Kotaki, M., & Ramakrishna, S. (2003). A review on polymer nanofibers by electrospinning and their applications in nanocomposites. *Composites Science and Technology*, *63*(15), 2223–2253. doi:10.1016/S0266-3538(03)00178-7
10. Santavirta, S., Takagi, M., Nordsletten, L., Anttila, A., Lappalainen, R., & Konttinen, T. (1998). C L I N I C A L A N D E X P E R I M E N TA L F O R U M Biocompatibility of silicon carbide in colony formation test in vitro A promising new ceramic THR implant coating material, 89–91.
11. Gao, F., Zheng, J., Wang, M., Wei, G., & Yang, W. (2011). Piezoresistance behaviors of p-type 6H-SiC nanowires. *Chemical communications (Cambridge, England)*, *47*(43), 11993–5. doi:10.1039/c1cc14343c
12. Choi, K., Choi, D. K., Lee, D.-Y., Shim, J., Ko, S., & Park, J. H. (2012). Preparation and application of the 3C–SiC substrate to piezoelectric micro cantilever transducers. *Applied Physics A*, *108*(1), 161–170. doi:10.1007/s00339-012-6866-x

13. Kudimi, J. M. R., Mohd-Yasin, F., & Dimitrijev, S. (2012). SiC-based Piezoelectric Energy Harvester for Extreme Environment. *Procedia Engineering*, *47*, 1165–1172. doi:10.1016/j.proeng.2012.09.359
14. Oliveros, A., Guiseppi-Elie, A., & Saddow, S. E. (2013). Silicon carbide: a versatile material for biosensor applications. *Biomedical microdevices*, 353–368. doi:10.1007/s10544-013-9742
15. González, P., Borrajo, J. P., Serra, J., Chiussi, S., León, B., Martínez-Fernández, J., Varela-Feria, F. M., et al. (2009). A new generation of bio-derived ceramic materials for medical applications. *Journal of biomedical materials research. Part A*, *88*(3), 807–13. doi:10.1002/jbm.a.31951
16. Zhu, D., Gao, M., Zhang, S., Wu, H., Pan, Y., Liu, Y., Pan, H., et al. (2012). A high-strength SiCw/SiC–Si composite derived from pyrolyzed rice husks by liquid silicon infiltration. *Journal of Materials Science*, *47*(12), 4921–4927. doi:10.1007/s10853-012-6365-7
17. Li, J., Zhang, Y., Zhong, X., Yang, K., Meng, J., & Cao, X. (2007). Single-crystalline nanowires of SiC synthesized by carbothermal reduction of electrospun PVP/TEOS composite fibres. *Nanotechnology*, *18*(24), 245606. doi:10.1088/0957-4484/18/24/245606
18. Eick, B. M., & Youngblood, J. P. (2008). SiC nanofibers by pyrolysis of electrospun preceramic polymers. *Journal of Materials Science*, *44*(1), 160–165. doi:10.1007/s10853-008-3102-3
19. Patel, N., Kawai, R., & Oya, A. (2004). Preparation of silicon carbide nanofibers by use of polymer, *9*, 691–693.
20. Vincent, M., Kim, M. S., Carraro, C., & Maboudian, R. (2012). SILICON CARBIDE NANOWIRES AS AN ELECTRODE MATERIAL FOR Berkeley Sensor & Actuator Center , 2 Department of Chemical and Biomolecular Engineering, (February), 39–42.
21. Carbon, C., Korenblit, Y., Rose, M., Kockrick, E., Borchardt, L., Kvit, A., Kaskel, S., et al. (2010). High-Rate Electrochemical Capacitors, *4*(3), 1337–1344.
22. So, K. P., Jeong, J. C., Park, J. G., Park, H. K., Choi, Y. H., Noh, D. H., … Lee, Y. H. (2013). SiC formation on carbon nanotube surface for improving wettability with aluminum. *Composites Science and Technology*, *74*, 6–13. doi:10.1016/j.compscitech.2012.09.014
23. Morisada, Y., Miyamoto, Y., Takaura, Y., Hirota, K., & Tamari, N. (2007). Mechanical properties of SiC composites incorporating SiC-coated multi-walled carbon nanotubes. *International Journal of Refractory Metals and Hard Materials*, *25*(4), 322–327. doi:10.1016/j.ijrmhm.2006.08.005
24. Morisada, Y., & Miyamoto, Y. (2004). SiC-coated carbon nanotubes and their application as reinforcements for cemented carbides. *Materials Science and Engineering: A*, *381*(1-2), 57–61. doi:10.1016/j.msea.2004.03.055
25. König, K., Novak, S., Ivekovič, A., Rade, K., Meng, D., Boccaccini, A. R., & Kobe, S. (2010). Fabrication of CNT-SiC/SiC composites by electrophoretic deposition. *Journal of the European Ceramic Society*, *30*(5), 1131–1137. doi:10.1016/j.jeurceramsoc.2009.07.027
26. Gu, X., Qiang, Y., & Zhao, Y. (2011). Synthesis, structural and electrical properties of SiC nanowires via a simple CVD method. *Journal of Materials Science: Materials in Electronics*, *23*(5), 1037–1040. doi:10.1007/s10854-011-0543-2

27. Mceachin, Z., & Lozano, K. (2012). Production and Characterization of Polycaprolactone Nanofibers via Forcespinning TM Technology, (May 2011). doi:10.1002/app
28. Takeda, M., Sakamoto, J., Imai, Y., & Ichikawa, H. (1999). Thermal stability of the low-oxygen-content silicon carbide ® ber ,, *59*, 813–819.
29. DiCarlo, Jim. "SiC Fiber Technology Status" PowerPoint presentation. SiC Fiber Forum, Dayton, OH. 15 Dec 2009.
30. Bunsell, a. R., & Piant, a. (2006). A review of the development of three generations of small diameter silicon carbide fibres. *Journal of Materials Science*, *41*(3), 823–839. doi:10.1007/s10853-006-6566-z
31. NASA website http://www.grc.nasa.gov/WWW/RT/RT2001/5000/5100dicarlo1.html
32. Steiner, D. (1998). . *Journal of Nuclear Materials*, *253*, 67–77.
33. Takeda, M., Urano, A., Sakamoto, J., & Imai, Y. (1998). Microstructure and oxidative degradation behavior of silicon carbide ® ber Hi-Nicalon type S. *Journal of Nuclear Materials*, *263*, 1594–1599.
34. Iveković, A., Novak, S., Dražić, G., Blagoeva, D., & de Vicente, S. G. (2013). Current status and prospects of SiCf/SiC for fusion structural applications. *Journal of the European Ceramic Society*, *33*(10), 1577–1589. doi:10.1016/j.jeurceramsoc.2013.02.013
35. Yen, G. V. (1988). Mechanical properties and structure of a commercial SiC-type fibre (Tyranno). *Journal of Materials Science*, *23*, 987–993.
36. Takeda, M., Sakamoto, J., Imai, Y., & Ichikawa, H. (1999). Thermal stability of the low-oxygen-content silicon carbide ® ber ,. *Composites Science and Technology*, *59*, 813–819.
37. Steiner, D. (1998). ž. *Journal of Nuclear Materials*, *253*, 67–77.
38. DERRICK, MICHELE R. "SOME NEW ANALYTICAL TECHNIQUES FOR USE IN CONSERVATION." *Journal of the American Institute for Conservation* 8th ser. 33.3 (1994): 171-83. Print.
39. *High Resolution TGATM (Hi-Res TGA)*. N.d. Photograph. Department Polimeri ICECHIM, Rominia.
40. *EDS Detector*. N.d. Photograph. Http://www.webanswers.com/post-images/D/DA/2E835DA2-911E-4801-95D36D559171066F.jpg, n.p.
41. Al-Jassim, Mowafak. *TEM EDS Reveals a Mixture of PbSe and PbTe Nanoparticles Present on Carbon Support Film Cu Grid.* 2013. Photograph. National Renewable Energy Laboratory, n.p.
42. *X-Ray Diffraction (XRD) and Fluorescence (XRF)*. 2009. Photograph. Advanced Nanofabrication Imaging and Characterization, Thuwal, Saudi Arabia.
43. Zhang, Y., Zhu, F., Zhang, J., & Xia, L. (2008). Converting Layered Zinc Acetate Nanobelts to One-dimensional Structured ZnO Nanoparticle Aggregates and their Photocatalytic Activity. *Nanoscale Research Letters*, *3*(6), 201–204. doi:10.1007/s11671-008-9136-2
44. Menard, Kevin P. *Dynamic Mechanical Analysis: A Practical Introduction*. Boca Raton, FL: CRC, 1999. Print.
45. Mathers, Patrick T., Prof. *DMA Q800 TA Instruments*. 2007. Photograph. Syracuse University, Syracuse, NY.
46. "Dynamic Mechanical Analysis." *Wikipedia*. Wikimedia Foundation, 09 June 2013. Web. 06 Nov. 2013.
47. "Polystyrene." *Polystyrene*. N.p., n.d. Web. 06 Nov. 2013.

48. "Sigma-Aldrich." *Sigma-Aldrich*. N.p., n.d. Web. 06 Nov. 2013.
49. Patlan, Richard. "FABRICATION AND CHARACTERIZATION OF POLYLACTIC ACID AND POLYLACTIC ACID / MULTI-WALLED CARBON NANOTUBE NANOFIBERS THROUGH CENTRIFUGAL SPINNING." Thesis. The University of Texas Pan-American, 2012. Print.
50. Periodicals, W. (2009). Mistakes Encountered During Automatic Peak Identification of Minor and Trace Constituents in Electron-Excited Energy Dispersive X-Ray Microanalysis, *31*(April), 1–11. doi:10.1002/sca.20151
51. Stefanaki, E. (2008). Electron Microscopy : The Basics, 1–11.
52. "Energy-Dispersive X-Ray Spectroscopy (EDS)." *Energy-dispersive Detector (EDS)*. N.p., n.d. Web. 26 Nov. 2013.
53. Diffraction, X., & Sources, I. (n.d.). Bragg ' s Law.
54. Sarkar, K., Gomez, C., Zambrano, S., Ramirez, M., de Hoyos, E., Vasquez, H., & Lozano, K. (2010). Electrospinning to Forcespinning^{TM}. *Materials Today*, *13*(11), 12–14. doi:10.1016/S1369-7021(10)70199-1

BIOGRAPHICAL SKETCH

Alfonso Salinas was born in Monterrey, Nuevo Leon, Mexico on March 7, 1989. After graduating from McAllen High School in 2007 he attended The University of Texas Pan American (UTPA), where he received his Bachelors of Science in 2011. While an undergraduate, he was involved in many student organizations such as Society of Hispanic Professional Engineers (SHPE), American Society of Mechanical Engineers (ASME), and Society of Manufacturing Engineers (SME). In his last semester as an undergraduate Alfonso, took a position as a research assistant in Dr. Lozano's PREM team, where his research focused on the development of polymeric nanofibers utilizing the Forcespinning® method. For correspondence, email salinas_20042@mns.com.